

# PixVerve: Advancing Native UHR Image Generation to 100MP with a Large-Scale High-Quality Dataset

Haojun Chen<sup>1,\*</sup>, Haoyang He<sup>1,\*</sup>, Chengming Xu<sup>2,\*</sup>, Qingdong He<sup>1</sup>, Junwei Zhu<sup>3</sup>, Yabiao Wang<sup>1</sup>, Zhucun Xue<sup>1</sup>, Xianfang Zeng<sup>1</sup>, Zhennan Chen<sup>3</sup>, Xiaobin Hu<sup>4</sup>, Hao Zhao<sup>5</sup>, Yong Liu<sup>1</sup>, Jiangning Zhang<sup>1,†,✉</sup>, Dacheng Tao<sup>6</sup>

<sup>1</sup>Zhejiang University, <sup>2</sup>Fudan University, <sup>3</sup>Nanjing University, <sup>4</sup>National University of Singapore, <sup>5</sup>Tsinghua University, <sup>6</sup>Nanyang Technological University

\*Joint first authors, †Corresponding author

Text-to-Image (T2I) models have recently seen notable progress around 1K and 2K resolution. With the extreme desire for better visual experience and the rapid development of imaging technology, the demand for Ultra-High-Resolution (UHR) image generation has grown significantly. However, UHR image generation poses great challenges due to the scarcity and complexity of high-resolution content. In this paper, we first introduce PixVerve-95K, a high-quality, open-source UHR T2I dataset curated with a carefully designed data pipeline, which contains 95K images across diverse scenarios (each image has a minimum pixel-count of 100M) and seven-dimensional annotations. Based on our large-scale image-text dataset, we take a pioneering step to extend various T2I foundation models to native 100MP generation with three training schemes. Finally, leveraging both conventional metrics and multimodal large language model-based assessments, our proposed PixVerve-Bench benchmark establishes a comprehensive evaluation protocol for UHR images encompassing visual quality and semantic alignment. Extensive experimental results on our benchmark and the constructive exploration of training strategies collaboratively provide valuable insights for future breakthroughs.

**Date:** May 20, 2026

**✉ Correspondence:** [186368@zju.edu.cn](mailto:186368@zju.edu.cn)

**Code:** <https://github.com/HaojunChen663/PixVerve-95K>

**Data:** <https://modelscope.cn/datasets/APRIL6AIGC/PixVerve-95K>

**Project:** <https://haojunchen663.github.io/projects/PixVerve/>



## 1 Introduction

In recent years, Text-to-Image (T2I) models have made remarkable advancements in synthesis quality and controllability [4, 29], underscoring their exceptional potential to revolutionize the paradigm of content creation. Despite substantial progress, most existing models focus on training and generation at fixed low-to-moderate resolutions (typically 1K and 2K). Directly extrapolating these models to Ultra-High-Resolution (UHR) scenarios inevitably leads to degradations such as structural artifacts, content repetition, and a pervasive loss of high-frequency details (see Fig. 2, top-right), which significantly hinder real-world applications that necessitate photorealistic visual fidelity.

With the extreme desire for better visual experience of the next-generation media [22, 52, 53, 57, 62] and empowered by computing resources, the demand for high-quality gigapixel-scale content has grown continuously in fields such as digital cinematography, immersive entertainment, and commercial design. Additionally, recent advancements in imaging technology and display devices have driven native 100-Megapixel (100MP) imaging a standard specification in modern smartphones of many brands and no longer confined to specialized domains. Furthermore, the theoretical resolution of the Human Visual System (HVS) is estimated to be 576 megapixels when integrating information across the 120-degree field of view [10]. This capacity implies that 100MP T2I generation is not merely a pursuit of larger dimensions, but a valuable quest to bridge the gap between digital synthesis and human perception. To this end, this work seeks to first advance UHR image generation to 100MP.

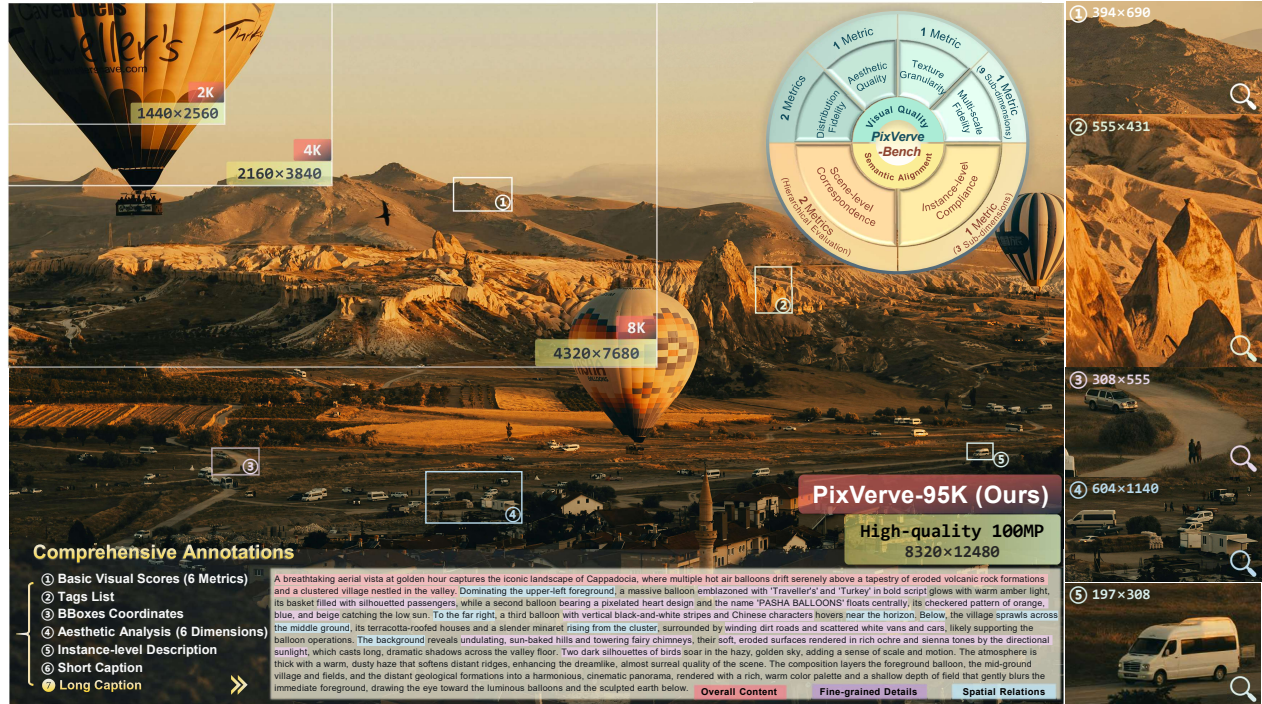


**Figure 1** PixVerve-95K is a large-scale, high-quality dataset for Ultra-High-Resolution (UHR) image generation, first advancing Text-to-Image (T2I) generation to the 100MP scale. Featuring high visual fidelity (right) and comprehensive annotations (bottom), it can meet the growing demand for next-generation T2I applications. **PixVerve-Bench** is a comprehensive benchmark suite comprising 8 metrics for the systematic evaluation of UHR T2I methods (top-right).

Recently, training-based methods for native image generation have demonstrated promising results at the 4K (~16MP) resolution [55, 58, 59, 61]. Compared to training-free strategies [3, 11, 12, 23] which often exhibit excessive smoothing and implausible details (see Fig. 2, bottom-left), these approaches enable model backbones to explicitly capture the long-range correlations within UHR images, thus attaining better performance in detail synthesis. However, extending UHR image generation to native 100MP is not simply about resolution scaling and faces three core challenges: **1)** The primary bottleneck for native 100MP T2I training and generation lies in the lack of suitable data. Existing UHR T2I datasets are modest in resolution (typically limited to 4K [59, 61]) due to the data scarcity and the difficulty in curating suitable data. Furthermore, public image-text corpora lack specialized captioning protocols for the UHR setting and rarely provide multi-dimensional, structured annotations which benefit precise control over various visual attributes. **2)** The immense semantic complexity and vast pixel space of 100MP data make it challenging to design effective training schemes, which is largely unexplored in the current landscape. **3)** Standard T2I evaluation protocols are inadequate for UHR scenarios, making it difficult to provide reliable feedback for training and model selection, as conventional metrics such as FID [20] and CLIPScore [19] fail to capture fine-grained details.

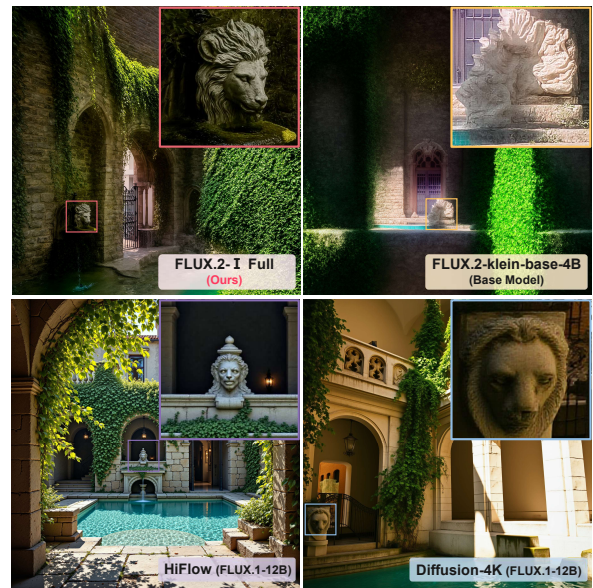


**Figure 2** Visual comparison of 4K image generations. Please zoom in for clearer details.

To bridge multi-faceted gaps, we propose a comprehensive methodology framework spanning dataset, model, and benchmark. Concretely, our core contributions are threefold:

- We introduce **PixVerve-95K**, the first large-scale, high-quality T2I dataset to push image resolution to 100MP. With a five-stage, automated data pipeline, we curate 95,735 100MP images with fine-grained annotations (5 types of metadata and 2 comprehensive captions), directly supporting the training or fine-tuning of T2I models at high resolutions.
- Based on our proposed PixVerve-95K, we first explore the attempt of generating 100MP images natively. Specifically, we extend existing T2I foundation models (including both latent diffusion models and pixel diffusion models) with three distinct training schemes, providing valuable insights and paving the way for future breakthroughs.
- To address the limitations of conventional T2I benchmarks, we construct **PixVerve-Bench**, a systematic, hierarchical evaluation protocol incorporating both traditional metrics and assessments based on Multimodal Large Language Models (MLLMs).

## 2 Related Work

### 2.1 Text-to-Image Datasets

The evolution of Text-to-Image (T2I) generation has been fundamentally driven by the availability and quality of large-scale image-text datasets. The release of the early web-scale corpora such as LAION-400M [41] and LAION-5B [42] has significantly facilitated T2I foundation model training. As the field further matures, the focus of dataset construction starts to shift from mere volume toward high quality [27]. With the growing demand for higher resolution and visual fidelity, Diffusion-4K [59] introduces the first open-source 4K T2I dataset for native UHR image training. More recently, Aesthetic-Train-V2 [58] and UltraHR-100K [61] further expand the 4K T2I corpora. Despite these advances, most existing datasets are primarily constrained to the 1K-4K regime and often rely on global, superficial descriptions that lack the structural granularity and instance-level detail required to supervise the synthesis of exceptionally complex Ultra-High-Resolution (UHR) scenes.

### 2.2 Text-to-Image Foundation Models

Mainstream T2I foundation models include the Generative Adversarial Network (GAN) [15], autoregressive (AR) models [37], and diffusion models (DMs) [21]. With this evolution of architectures, DMs have recently emerged as the prevailing paradigm, pushing T2I generation to an unprecedented level [28, 29, 32, 40, 45, 50]. A pivotal milestone is the introduction of latent diffusion models (LDMs) [40], which perform the diffusion process in a compressed latent space, alleviating computational burdens while maintaining high perceptual fidelity [13, 35]. More recently, Diffusion Transformers (DiTs) [34] have made remarkable progress within the LDM framework, offering superior scalability compared to traditional U-Net backbones. Parallel to the paradigm of LDMs, pixel diffusion models perform the diffusion process directly in the raw pixel space, which have regained attention for image generation these days [7, 8, 31, 48]. While LDMs are often preferred for their computational efficiency at moderate resolutions, pixel diffusion models offer a distinct advantage by bypassing the potential information loss and reconstruction artifacts inherent in Variational Autoencoder-based compression. Nevertheless, most current T2I foundation models are constrained to fixed low-to-moderate resolutions (typically  $1024 \times 1024$ ), leaving UHR T2I generation a relatively under-explored field.

### 2.3 Ultra-High-Resolution Image Generation

Beyond the 2K resolution threshold, image generation is currently dominated by LDMs. Existing solutions can be categorized into two main paradigms: training-free strategies for UHR scaling [3, 11, 18, 23, 44] and training-based methods for native UHR image generation [6, 39, 46, 55, 58, 59, 61]. Despite being more resource-friendly, the former approaches often suffer from object repetition, texture degradation, and unrealistic details. To enhance synthesis quality, the alternative direction curates UHR T2I corpora and trains or fine-tunes models at native high resolutions. However, current training-based frameworks remain

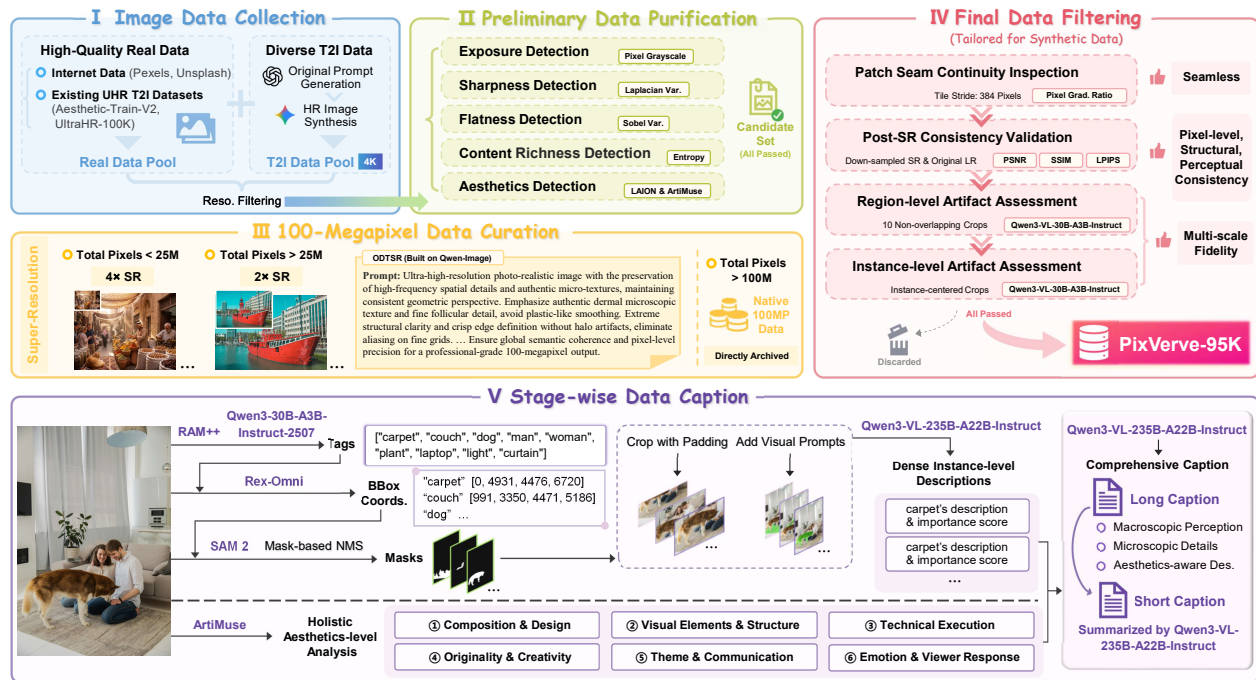


**Figure 3** Overview of our **PixVerve-95K** curation pipeline that includes: **1)** High-quality and diverse raw image data acquisition (Sec. 3.1.1). **2)** Preliminary data purification comprising five parallel detection procedures (Sec. 3.1.2). **3)** 100MP data curation via super-resolution (Sec. 3.1.3). **4)** Final data filtering to ensure the quality of our synthetic data (Sec. 3.1.4). **5)** Stage-wise data caption pipeline carefully designed for UHR images (Sec. 3.1.5).

confined to the sub-4K [6] or 4K [55, 58, 59, 61] scale, still falling short of the gigapixel-scale fidelity required for real-world applications. In this paper, we aim to take a pioneering step and push the frontier of T2I to the 100MP scale.

### 3 Methodology: Dataset, Model, and Benchmark

In this work, we operationalize **Native 100MP Text-to-Image Generation** as a dedicated training and evaluation regime, significantly distinct from approaches of training-free resolution upscaling. Training-based methods treat UHR image generation as an end-to-end task that requires intrinsic high-resolution priors, while executing this regime necessitates addressing two fundamental challenges: **i) high-quality 100MP T2I datasets and ii) training recipes**. Also, the absence of a systematic T2I benchmark designed for UHR scenarios hinder further research on this valuable topic. Resolving these challenges requires a holistic methodology that integrates data, model training, and evaluation.ression.

#### 3.1 Curating PixVerve-95K Dataset

To facilitate direct training at native 100MP resolution, we curate the first large-scale 100MP T2I dataset, addressing the critical deficit of UHR corpora in the current landscape. Beyond the pursuit of extreme resolution, we prioritize high image quality and caption comprehensiveness. To this end, we carefully design and implement a five-stage data pipeline, which is intuitively shown in Fig. 3.

##### 3.1.1 Raw Image Data Collection

**High-quality real data collection.** To establish a large-scale image corpus for UHR T2I generation, we begin by collecting high-resolution real imagery from diverse sources. We harvest high-quality photography from platforms Pexels [25] and Unsplash [9] via official APIs, while also integrating a subset from Aesthetic-Train-V2 [58] and UltraHR-100K [61]. Both data collection streams are subjected to a deduplication procedure and

notably, we apply the following resolution-based screening criteria to construct a data pool prior to 100MP upscaling: *i)* total pixels exceeding 25M with a minimum dimension of 3,000 pixels, or *ii)* total pixels ranging from 10M to 25M with a minimum dimension of 1,500 pixels. Detailed clarification on image licensing is provided in [Sec. C](#).

**Diverse T2I data generation.** To further enhance semantic diversity and ensure the comprehensiveness of visual concepts, we complement the real data with synthesized data. Specifically, we leverage GPT-5.1 [47] to generate a set of wide-ranging, expressive prompts, which are subsequently sent to the advanced Nano Banana Pro [16] to generate high-quality 4K images. Together with the real data, these diverse synthesized images constitute our raw data pool (approximately 300K).

### 3.1.2 Preliminary Data Purification

Large-scale image corpora collected from diverse sources inevitably contain subpar samples suffering from technical degradation (*e.g.*, exposure anomalies, blurriness, *etc.*), which can undermine the learning efficacy of T2I models. Therefore, to establish a baseline of visual excellence, we comprehensively evaluate each image in our raw data pool across five fundamental dimensions:

**Exposure detection.** Overexposure and underexposure degrade the image quality greatly. Taking 5 as the threshold, we calculate the cumulative proportion of pixels with values above 250 or below 5 for each image. Any image of which the proportion exceeds 20% is deemed anomalous and excluded.

**Sharpness detection.** To eliminate the presence of out-of-focus or motion-blurred images, we utilize the Laplacian variance as an interpretable metric for image sharpness assessment. Images yielding a score below the threshold of 10 are identified as insufficiently clear and discarded from the corpus.

**Flatness detection.** To suppress images dominated by textureless regions, we partition each image into local patches and compute the proportion of overly smooth patches based on the Sobel variance. Images are considered to severely lack texture and then removed if the proportion exceeds 97.5%.

**Content richness detection.** Beyond basic physical properties, superior content richness is another defining characteristic of a high-quality image. We employ the classical signal, Shannon entropy [43], to quantify the informational density, retaining the top 60% highest-entropy images in the raw pool.

**Aesthetics detection.** Aesthetic appeal plays an important role in high-quality image generation. For aesthetics detection, we adopt a coupling approach which combines the LAION Aesthetic Predictor [30] and ArtiMuse [5], a modern MLLM-based aesthetics evaluator. We utilize both predictors to assess the aesthetic quality of each image in the raw pool with the score  $S_L$  and  $S_A$  respectively. Images of which  $S_L$  or  $S_A$  ranks among the top 60% are preserved.

By taking the intersection of the subsets retained from the five detection procedures above, the final candidate pool is derived.

We present representative discarded and qualified examples for each dimension along with their corresponding scores in [Fig. 4](#), demonstrating the necessity and effectiveness of our preliminary data purification.

### 3.1.3 100MP Data Curation

Given the scarcity of native 100MP image data in our candidate pool, we employ ODTSR [14], a novel super-resolution (SR) framework based on Qwen-Image [50] which considers both fidelity and controllability, to bridge this gap and expand the scale of our final corpus. Notably, we employ a tiling strategy to tackle the high-resolution nature, which incorporates overlapping strides and feathering matrices to facilitate smooth

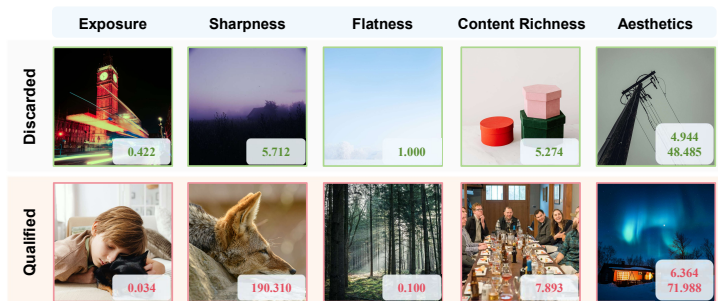


**Figure 4** Representative discarded and qualified examples for each dimension. Green scores represent disqualification, while red scores represent passing the detection.

**Table 1** Data Flow and Refinement Details.

Pipeline Stage	Resulting Subset	Scale
Image Data Collection	Raw Data Pool	300,316 (5,000 Synthesized Images)
Preliminary Data Purification	Candidate Data Pool	122,866
Final Data Filtering	Final Data	95,935 (95,735+200)

transitions. We implement distinct upscaling intensities for different source resolutions to reach the uniform 100MP threshold, leveraging textual prompts as conditional guidance: **i)** native 100MP images are directly archived; **ii)** images with a total pixel count exceeding 25M are elevated via  $2\times$  SR; and **iii)** for the remaining images with total pixels in the 10M-25M range, a  $4\times$  SR process is performed. This tiered production pipeline ensures that all samples achieve a minimum resolution of 100MP with high perceptual fidelity, establishing a sound data foundation for UHR T2I training and generation.

### 3.1.4 Final Data Filtering

To guarantee the quality of our synthetic 100MP data, we rigorously implement a four-tiered filtering pipeline, which specially targets different problems potentially introduced during the SR process.

**Patch seam continuity inspection.** To eliminate color discontinuities and geometric misalignments, we compute the pixel gradient ratio across all horizontal and vertical seams defined by the 384-pixel tile stride used in [Sec. 3.1.3](#). An image is considered defective and strictly excluded if any detected seam exhibits a ratio exceeding the threshold  $r_t = 2.5$ .

**Post-SR consistency validation.** To ensure pixel-level, structural, and perceptual fidelity, each synthetic 100MP image is down-sampled to its original resolution and compared against its initial input via Peak Signal-to-Noise Ratio (PSNR), Structural Similarity Index (SSIM), and LPIPS [60]. Any candidate image that fails to satisfy the tri-metric thresholds is consequently discarded.

**Region-level artifact assessment.** To prevent local degradations such as geometric deformations and warped human features, we partition each synthetic 100MP image into non-overlapping patches of size 768 and employ a hybrid sampling strategy to select ten representative patches: six with the highest texture complexity (via the Sobel variance) and the remaining four sampled randomly. All selected patches are then evaluated by Qwen3-VL-30B-A3B-Instruct [1]. An image is strictly discarded if more than one of its sampled patches is identified as containing noticeable artifacts.

**Instance-level artifact assessment.** We further scrutinize key instances leveraging the image crops obtained in [Sec. 3.1.5](#). Similarly, we employ Qwen3-VL-30B-A3B-Instruct [1] to evaluate each crop, adopting a stringent criterion where an image is excluded if any instance is flagged as defective.

[Tab. 1](#) illustrates the specific data flow and the data scale at each major stage, tracing the refinement process from the initial collection to the final curated corpus.

### 3.1.5 Stage-wise Data Caption

Detailed captions are crucial for fine-grained controllable image generation, which is widely recognized [2, 55, 61]. However, standard zero-shot MLLM prompting often fails to encapsulate the intricate details present in UHR images. To address this challenge, we propose a hierarchical stage-wise pipeline which decouples the captioning process into three distinct layers:

**Dense instance-level descriptions generation.** To facilitate precise alignment at the instance level, we design a cascaded pipeline utilizing the capabilities of foundation models and MLLMs. We first employ RAM++ [24] for open-vocabulary tagging to generate semantic tags, which are pruned by Qwen3-30B-A3B-Instruct-2507 [54] to retain only tangible object tags. Rex-Omni [26] predicts bounding boxes (bboxes) for these filtered tags, followed by a step where SAM 2 [38] performs instance segmentation and generates high-fidelity masks. We further apply Non-Maximum Suppression (NMS) based on IoU to deduplicate overlapping masks and remove trivial objects with an area threshold. For context-aware captioning, we generate a visual pair

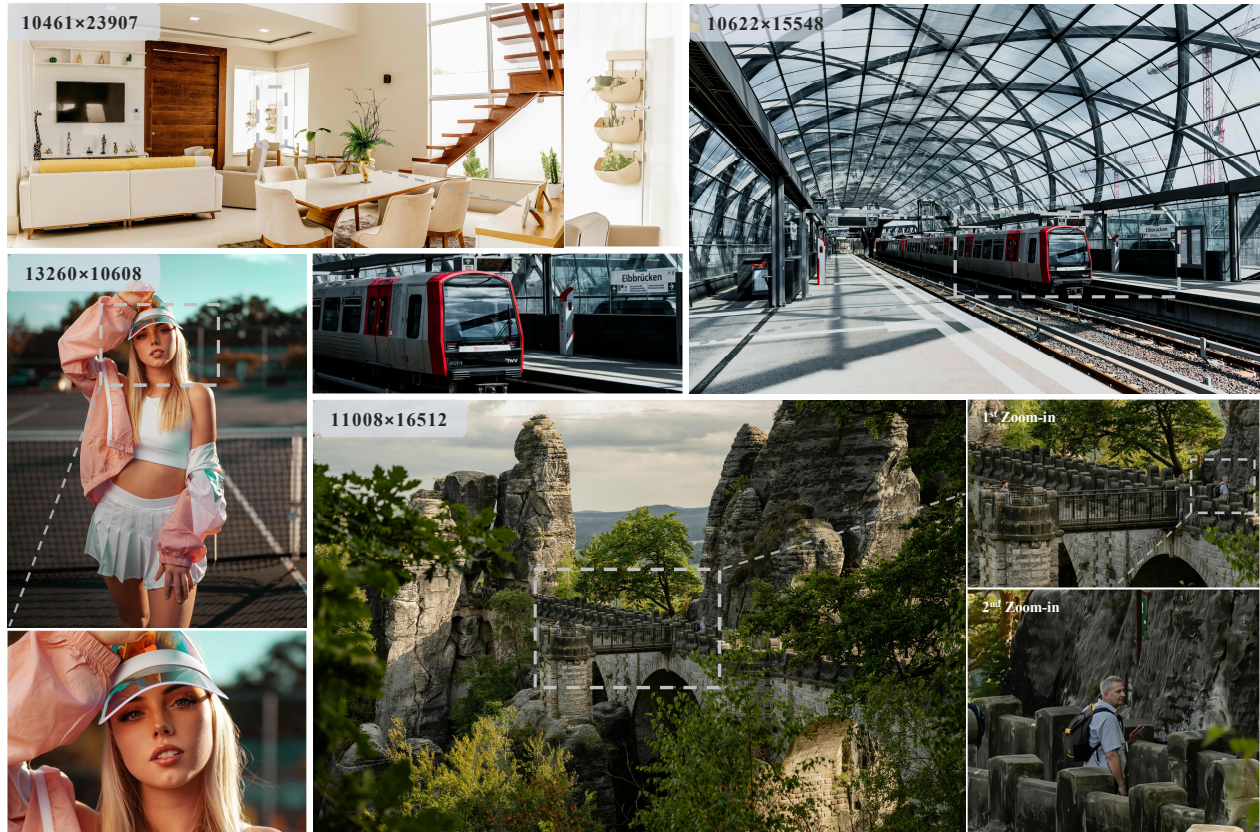


**Figure 5** Qualitative samples in our PixVerve-95K dataset. The zoomed-in regions highlight the fine-grained and high-fidelity details.

for each identified instance. Specifically, we crop out a sub-image centered on the target instance with 5% padding and incorporate a highlighted prompt on the original image using its mask. These visual pairs are finally sent to Qwen3-VL-235B-A22B-Instruct [1] to generate comprehensive instance-level descriptions and assign a semantic importance score to each instance.

**Holistic aesthetics-level analysis.** Beyond instance details, a high-quality image caption should encompass an aesthetic depiction spanning multiple dimensions. To this end, we adopt ArtiMuse [5] to provide an expert-style aesthetic analysis across six key dimensions (composition & design, visual elements & structure, technical execution, originality & creativity, theme & communication, and emotion & viewer response), which serves as a vital reference for final caption summarization.

**Comprehensive caption summarization.** Based on key instances’ detailed descriptions and the aesthetic analysis, we employ Qwen3-VL-235B-A22B-Instruct [1] as a caption synthesis expert. With the original image and all aggregated metadata, it first generates a coherent long caption encompassing the overall content and style, fine-grained details of instances, and clear relations between objects (as shown in Fig. 1). Paired with the original image, this long caption is subsequently distilled by the same MLLM into a short caption that encapsulates the core semantic essence in a concise and fluid narrative, which can meet diverse task requirements together with the long version.

### 3.1.6 Statistical Comparison and Analysis

With our five-stage data pipeline, we construct **PixVerve-95K**, comprising 95,735 100MP images with comprehensive annotations. Fig. 5 presents some qualitative samples, which are best viewed zoomed-in. As summarized in Tab. 2, PixVerve-95K is the first to push open-source T2I data to 10K resolution ( $\sim 100$ MP), providing five-dimensional metadata (basic visual scores, tags, bboxes, aesthetics-level analysis, and instance-level description) beyond long and short captions. These structured annotations offer versatile utility for the

**Table 2** Comparison with open-source UHR T2I datasets. Our proposed **PixVerve-95K** is the first premium T2I dataset to push image resolution to 10K ( $\sim 100\text{MP}$ ), providing multi-dimensional, fine-grained metadata and significantly longer comprehensive captions.

Dataset	Avg. Resolution (height $\times$ width)	Number	Avg. Caption Length	Basic Visual Scores	Tags	BBoxes	Aesthetics-level Analysis	Instance-level Description	Variable-length Caption
PixArt-30k [6]	2531 $\times$ 2656	30,000	71.3 words	$\times$	$\times$	$\times$	$\times$	$\times$	$\times$
Aesthetic-Train [59]	4578 $\times$ 4838	12,015	24.2 words	$\times$	$\times$	$\times$	$\times$	$\times$	$\times$
Aesthetic-Train-V2 [58]	4861 $\times$ 5127	105,288	38.1 words	$\times$	$\times$	$\times$	$\times$	$\times$	$\times$
UltraHR-100K [61]	3654 $\times$ 5143	100,486	109.2 words	$\times$	$\times$	$\times$	$\times$	$\times$	$\times$
<b>PixVerve-95K (Ours)</b>	<b>13031 <math>\times</math> 15348</b>	95,735	234.1 words (Long)	$\checkmark$ (6 Metrics)	$\checkmark$	$\checkmark$	$\checkmark$ (6 Dimensions)	$\checkmark$	$\checkmark$

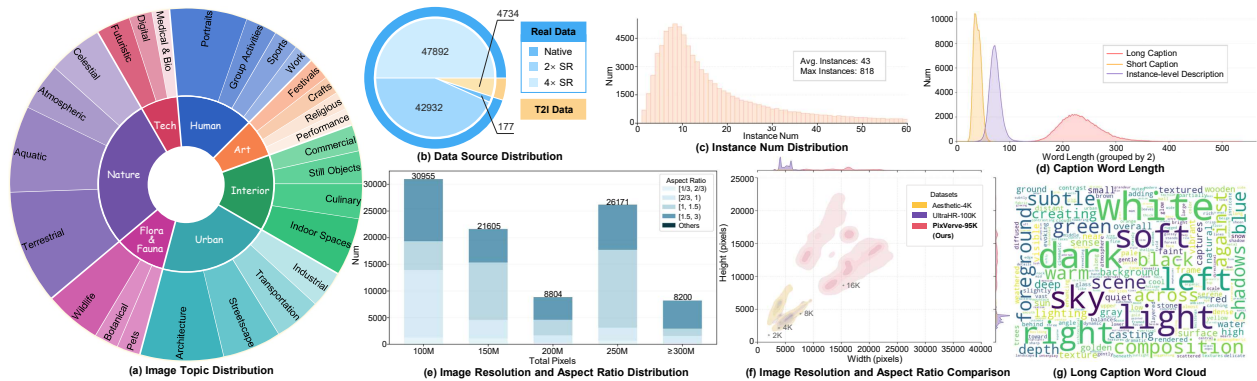


**Figure 6** Statistical distributions of our PixVerve-95K.

community, enabling granular control over data quality and facilitating adaptive sampling strategies tailored to specialized training objectives. Fig. 6 visualizes the statistical distributions of PixVerve-95K from multiple perspectives, highlighting the scenario diversity, balanced aspect ratios, and the exceptional expressiveness of aggregated captions.

### 3.2 Extending Text-to-Image Foundation Models to Native 100MP Generation

Training T2I foundation models at native 100MP poses great challenges due to the immense semantic complexity and vast pixel space. Bridging this gap necessitates a collaborative exploration of diverse architectural and optimization strategies rather than a singular fix. Based on PixVerve-95K, we conduct a multi-faceted exploration to retrofit T2I foundation models for native 100MP synthesis. Specifically, we investigate three distinct schemes to identify the optimal path:

- Scheme I: Full-Attention LDM Fine-tuning.** As direct baselines, we perform full-parameter training and use LoRA for parameter-efficient fine-tuning (PEFT) on FLUX.2-klein-base-4B [29], respectively. While maximizing the retention of the pre-trained model’s semantic prior and structural integrity, this approach encounters severe hardware constraints. The latent representation dimensions lead to an exponential surge in memory requirements, mandating model parallelism for inference at the 100MP scale, which limits the flexibility for general-purpose deployment in real world.
- Scheme II: Window-Attention Retrofitting and LDM Fine-tuning.** Inspired by EMOv2 [56], we refine the training strategy by introducing a local-to-global attention mechanism. We retrofit the joint attention in FLUX.2 into a dual-branch window-attention, without altering the core architecture of full-attention pretrained models. Specifically, text queries attend to all text and image tokens, while each image query attends to all text tokens and two complementary image-token neighborhoods. The close branch partitions the latent grid into contiguous spatial windows, preserving high-frequency local structure; while the remote branch groups tokens with the same modulo offset under the same partition stride, providing sparse long-range communication across the canvas. The outputs of the close and remote branches are averaged to approximate the original full image attention. For a latent grid consisting of  $N = HW$  image tokens, a

standard full self-attention mechanism incurs a quadratic computational cost of  $\mathcal{O}(N^2)$ . By retrofitting the attention with partition factors  $(a, b)$ , this scheme effectively reduces the image-image attention complexity to approximately  $\mathcal{O}(2N^2/(ab))$ , while the complexity for text-image conditioning remains linear with respect to  $N$  since the number of text tokens is small. Following T3-Video [57], we further cycle layer-wise partition schedules with different window size so different blocks exchange information under different receptive-field shapes.

- Scheme III: Patch-based Diffusion in Pixel Space.** Motivated by recent pixel diffusion models [7, 8, 31], we explore a paradigm bypassing the latent space entirely. Following L2P [8], which is built on DiP [7], we adopt a patch-based pixel diffusion framework that decouples global structure from local refinement: a transformer backbone operates on large image patches for long-range semantics and spatial layout, while a lightweight head leverages contextual features and original noisy patches to reconstruct fine details. From the theoretical perspective of L2P, large-patch tokenization preserves global low-frequency information efficiently, but high-frequency components are only weakly recovered during denoising unless explicit local inductive bias is introduced, making dedicated patch refinement crucial for faithful pixel-space reconstruction. However, scaling this scheme to UHR scales exposes a severe sequence-length and memory bottleneck. To enable training on a single 96 GB GPU card, we adaptively adjust the patch size to control the token count at the cost of coarser patch-level representations at higher resolutions.

**Progressive Training Strategy.** To mitigate the training instability inherent in the transition from standard resolutions to 100MP, we implement a three-stage progressive training strategy across all schemes. Models are fine-tuned through three graduated resolution tiers: 4K ( $\sim 16$ MP), 8K ( $\sim 64$ MP), and finally the target 10K (100MP). Concretely, these constructive experimental routes collaboratively provide critical insights into the resolution scalability of current T2I foundation models.

### 3.3 PixVerve-Bench Construction and Evaluation

For systematic and universal evaluation of UHR T2I models, we introduce **PixVerve-Bench**, comprising 200 manually picked images across diverse scenarios with an average resolution of  $12369 \times 14377$ . The benchmark framework (see Fig. 1, top-right) leverages both conventional metrics and novel MLLM-as-a-judge protocols, providing a holistic evaluation across two complementary aspects: **1) Visual Quality Assessment**, comprising four critical dimensions, including distribution consistency, aesthetic quality, texture granularity, and multi-scale fidelity; and **2) Semantic Alignment Evaluation**, which assesses instructional adherence across scene-level correspondence and instance-centric compliance. Detailed evaluation procedures and scoring formulas are provided in Sec. F.

#### 3.3.1 Visual Quality Assessment

Visual Quality evaluates the intrinsic physical attributes and perceptual realism of the generated images across the following four dimensions:

**Distribution Consistency.** Following common practice, we employ FID [20] to evaluate the overall distribution fidelity of the generated images. Considering that FID is calculated on down-sampled ( $299 \times 299$ ) images and neglects details, we incorporate  $FID_{\text{patch}}$  to scrutinize local patches.

**Aesthetic Quality.** Utilizing the LAION Aesthetic Predictor [30], we map each generated image into an aesthetic feature space and score its aesthetic quality.

**Texture Granularity** focuses on the richness and complexity of micro-patterns, which are among the most significant characteristics of UHR images. Using the Gray Level Co-occurrence Matrix (GLCM) [17] Score, we provide a rigorous diagnosis of whether the generated images suffer from monotonous flatness. Higher scores indicate richer texture and greater details.

**Multi-scale Fidelity.** The fidelity of UHR images is susceptible to both global artifacts (*e.g.*, structural incoherence and physical distortion) and local artifacts (*e.g.*, unrealistic noise and pattern repetition), which are difficult to capture using conventional metrics. Therefore, we employ Qwen3.5-35B-A3B [36] to perform a rigorous multi-scale fidelity assessment. Specifically, we systematically categorize the UHR-specific artifacts into two main dimensions and nine fine-grained sub-dimensions. The model is instructed to assign a score on a

five-point scale for each sub-dimension based on the severity of the artifact, followed by a unifying step where these individual scores are integrated into an interpretable metric, the **Multi-scale Fidelity Index (MSFI)**, to reflect overall performance.

### 3.3.2 Semantic Alignment Evaluation

Semantic Alignment evaluates how well the generated visual content adheres to the provided textual prompts. Given the expansive canvas and semantic complexity in UHR T2I generation, we hierarchically assess instructional adherence across two levels of granularity:

**Scene-level Correspondence.** For this foundational granularity, we first utilize CLIPScore [19] to measure the global semantic correlation using the short captions. Furthermore, we incorporate FG-CLIP2 Score [51] to better capture fine-grained details, which is computed on the long captions.

**Instance-centric Compliance.** To complement global correlation metrics, we propose the **Instance-centric Compliance Score (ICS)**. ICS leverages the advanced capabilities of Qwen3.5-35B-A3B [36] to assess semantic alignment across three hierarchical dimensions: Instance Existence Verification, Appearance Attribute Alignment, and Spatial Relation Accuracy, which provides a fine-grained and interpretable metric for measuring whether visual elements adhere to textual prompts.

## 4 Experiments

### 4.1 Experimental Setup

**Overall training settings.** As introduced in Sec. 3.2, we investigate three training schemes in our experiments. **Scheme I:** We fine-tune the pretrained FLUX.2-klein-base-4B [29] model using both full-parameter tuning and LoRA adaptation. For full-parameter fine-tuning, the learning rate is fixed at  $1 \times 10^{-5}$  across all resolution tiers. For LoRA fine-tuning, we use a learning rate of  $1 \times 10^{-4}$  and set the LoRA rank to 32. **Scheme II:** For the window-attention retrofitting, we adopt window aspect ratios of 1:1, 1:2, 2:1, 1:8, and 8:1. The window size is scaled linearly with the input resolution. **Scheme III:** To enable training on a single 96 GB GPU card at different scales, we adjust the patch size used in L2P [8] accordingly. Specifically, the patch sizes are set to 64, 128, and 320 for 4K, 8K, and 10K resolution, respectively. Unless otherwise specified, the learning rate is uniformly set to  $5 \times 10^{-5}$ . More training details including the fine-tuning epochs and computational expenditures are provided in Sec. E.1.

**Baselines.** Corresponding with our proposed training schemes, we denote our fine-tuned variants as FLUX.2-I (Full), FLUX.2-I (LoRA), FLUX.2-II, and L2P-III, respectively. To comprehensively evaluate our approaches, we conduct extensive comparisons against different baselines across three UHR scales: 4K ( $4096 \times 4096$ ), 8K ( $8192 \times 8192$ ), and 10K ( $10240 \times 10240$ ). The compared methods encompass: **i)** direct extrapolation of pre-trained T2I models (FLUX.2-klein-base-4B [29], Qwen-Image [50], and L2P [8]), **ii)** representative training-free strategies (DemoFusion [11], LinFusion [33], and HiFlow [3]), and **iii)** recent training-based models (UltraPixel [39], UltraFlux [55], and Diffusion-4K [59]). All baselines are evaluated with their official implementations and parameter settings.

### 4.2 Experimental Results, Observations, and Analysis

Tab. 3 presents the quantitative performance across three different resolutions on PixVerve-Bench, with detailed sub-dimension performance of the MSFI shown in Tab. A4). Fig. 7 as well as Fig. 2 illustrates a qualitative comparison at 4K resolution. In this section, we report our key observations and analysis regarding the resolution scalability of current methods and different T2I foundation models.

**Base Model and Existing Methods.** Directly extrapolating the base model FLUX.2-klein-base-4B to UHR generation leads to severe degradation: at 8K, FID exceeds 422, and CLIPScore drops to 18.345. Training-free strategies such as DemoFusion [11] and LinFusion [33] can maintain relatively good local visual statistics beyond 4K, *e.g.*, DemoFusion obtains the best  $FID_{patch}$  at 8K and 10K. However, their performance on semantic alignment remains limited; DemoFusion achieves ICS below 3.7 across all resolutions, indicating

**Table 3 Quantitative comparison on PixVerve-Bench.** The best result is highlighted in **bold**, while the second-best result is underlined. – indicates complete failures such as producing meaningless textures or black images, which are not applicable to the semantics-agnostic GLCM Score and MSFI.

Resolution (height × width)	Method	Visual Quality					Semantic Alignment		
		FID ↓	FID <sub>patch</sub> ↓	Aesthetics ↑	GLCM Score ↑	MSFI ↑	CLIPScore ↑	FG-CLIP2 Score ↑	ICS ↑
<b>4K</b> (4096 × 4096)	FLUX.2-klein-base-4B [29]	167.234	76.794	5.498	0.873	7.408	31.058	17.049	5.376
	Qwen-Image [50]	140.740	53.200	5.707	0.611	8.293	33.041	18.492	6.753
	L2P [8]	126.089	90.803	5.852	0.818	6.904	33.890	19.501	7.954
	DemoFusion [11]	142.981	55.164	6.167	0.733	8.246	32.608	18.105	3.619
	LinFusion [33]	142.933	68.184	<b>6.302</b>	0.394	8.171	32.246	17.694	3.849
	HiFlow [3]	130.337	49.842	6.189	<b>1.068</b>	8.779	34.190	19.643	6.978
	UltraPixel [39]	144.859	66.878	<u>6.260</u>	0.732	<b>9.153</b>	32.430	17.836	3.741
	UltraFlux [55]	<u>121.337</u>	49.902	6.068	<u>1.037</u>	8.712	<b>34.909</b>	<b>20.084</b>	<u>8.530</u>
	Diffusion-4K [59]	134.702	78.323	5.848	0.668	8.377	33.421	18.749	6.423
	FLUX.2-I (Full)	128.897	<u>45.204</u>	5.804	0.987	8.911	34.161	19.683	<b>8.533</b>
	FLUX.2-I (LoRA)	127.436	<b>40.433</b>	5.798	0.977	<u>8.977</u>	34.178	<u>19.767</u>	8.420
	FLUX.2-II	161.729	76.460	5.530	0.593	8.125	31.663	18.119	5.340
L2P-III	<b>118.183</b>	98.704	5.792	0.896	6.990	<u>34.264</u>	19.676	7.870	
<b>8K</b> (8192 × 8192)	FLUX.2-klein-base-4B [29]	422.737	350.331	4.121	–	–	18.345	0.503	0.318
	L2P [8]	<u>140.396</u>	87.167	5.590	0.363	<u>7.592</u>	<b>33.261</b>	<b>18.548</b>	<b>6.394</b>
	DemoFusion [11]	176.068	<b>58.480</b>	<u>6.031</u>	<u>0.514</u>	6.966	31.529	17.057	2.122
	LinFusion [33]	143.429	<u>62.658</u>	<b>6.271</b>	0.177	<b>7.797</b>	32.097	17.530	3.809
	FLUX.2-I (Full)	197.690	66.571	5.289	–	–	28.676	10.765	0.420
	FLUX.2-I (LoRA)	277.410	99.414	4.752	–	–	24.250	8.086	0.411
L2P-III	<b>134.635</b>	133.453	5.569	<b>1.122</b>	5.310	<u>32.788</u>	<u>17.802</u>	<u>5.504</u>	
<b>10K</b> (10240 × 10240)	L2P [8]	<u>156.158</u>	116.379	5.438	0.533	<u>7.397</u>	<b>32.440</b>	<b>17.866</b>	<b>5.548</b>
	DemoFusion [11]	179.063	<b>61.854</b>	<u>5.895</u>	0.538	6.710	30.930	15.920	2.671
	LinFusion [33]	<b>152.964</b>	<u>70.718</u>	<b>6.215</b>	0.156	<b>7.525</b>	<u>31.937</u>	<u>17.380</u>	<u>4.825</u>
	L2P-III	159.212	192.286	5.569	<b>1.100</b>	5.567	31.810	17.057	3.586

that tiled or progressive inference struggles to preserve prompt consistency. At 4K, UltraFlux [55] is a strong baseline with FID 121.337 and ICS 8.530, but our FLUX.2-I achieves better local fidelity with lower FID<sub>patch</sub>.

**Scheme I: Strong 4K Adaptation but Poor Scalability.** Fine-tuning the base model with *Scheme I* achieves the best balance at 4K. Compared with the base FLUX.2-klein-base-4B, the LoRA variant reduces FID<sub>patch</sub> from 76.794 to 40.433, while the full-parameter variant improves ICS from 5.376 to 8.533. These results show that fine-tuning effectively adapts local image statistics while preserving the semantic prior. Qualitatively, it generates coherent layouts and fine details without over-sharpening or texture collapse. However, this advantage comes with heavy computational overheads. As shown in Tab. A1, full fine-tuning at 4K costs over 20,000 H2O GPU hours, and only 0.25 epoch at 8K costs over 10,000 GPU hours. Inference also scales poorly: Tab. A2 shows that FLUX.2-I variants require 8 GPUs and over 100s at 4K, over 1,200s at 8K, and nearly 3,000s at 10K. This confirms that full-attention LDM fine-tuning is effective at 4K but impractical for native 100MP synthesis.

**Scheme II: Faster Attention with Optimization Difficulty.** FLUX.2-II reduces computational cost through window-attention retrofitting. As shown in Tab. A2, the inference time at 4K is reduced by approximately 32s on 8 GPUs, giving 30% speedup. Its 4K training cost is also lower than that with *Scheme I*, requiring 9,216 H2O GPU hours for 3 epochs. However, we observe that performance drops noticeably: FLUX.2-II obtains FID<sub>patch</sub> 76.460 and ICS 5.340, close to the base model but much worse than both FLUX.2-I variants. This suggests a mismatch between the pretrained full-attention structure and the retrofitted local attention pattern. In practice, the model requires more optimization steps to recover global communication, and the final quality is sensitive to the window size and aspect-ratio schedules.

**Scheme III: Best Scalability with a Patch-Size Trade-off.** It is surprisingly observed that L2P-III shows the strongest scalability among our explored schemes. It achieves the best FID at 4K and 8K, with scores of 118.183 and 134.635, and remains functional at 10K. More importantly, Tab. A2 shows that L2P-III needs one GPU and 58s, 70s, and 88s for 4K, 8K, and 10K inference. Compared with DemoFusion, it is up to

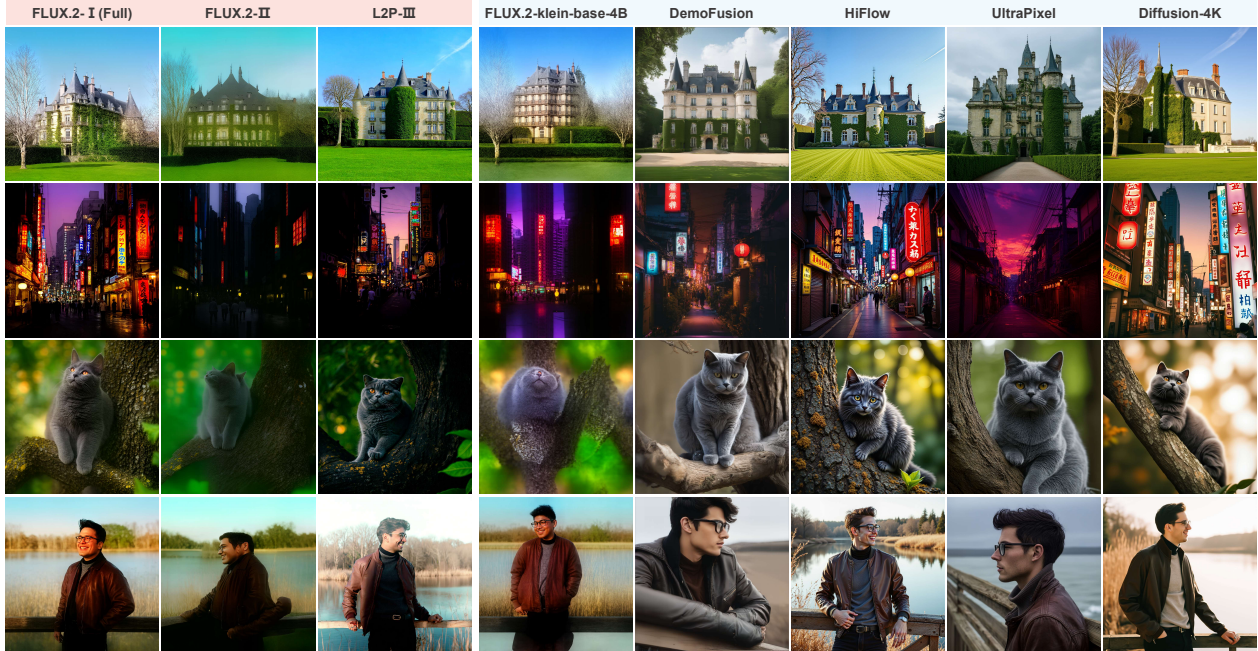


Figure 7 Qualitative comparison of different methods at 4K (4096×4096) resolution.

156× faster. Compared with FLUX.2-I LoRA at 10K, it is over 33× faster while using 1 GPU instead of 8. The main limitation is the patch-size trade-off: to fit training into a single 96 GB GPU card, the patch size increases from 64 to 128 and 320, reducing memory cost but weakening fine-detail reconstruction. This explains its less competitive  $FID_{patch}$  and MSFI at high resolutions. Overall, patch-based pixel diffusion is currently the most practical path toward native 100MP generation.

### 4.3 Ablation Study and Discussion

**Ablation on image caption quality.** We investigate the impact of caption granularity on image synthesis by comparing 4K image generations under short and long prompting settings on PixVerve-Bench. Evaluations across UltraFlux, Diffusion-4K, and FLUX.2-I (Full) reveal consistent performance gains when using long captions, as summarized in Tab. 4, indicating that increased descriptive granularity and semantic density are of great significance for UHR image generation. The visual comparison is shown in Fig. A4.

**Discussion on downstream applications.** Beyond T2I generation, our dataset supports diverse downstream tasks such as UHR image quality assessment, fine-grained understanding in UHR contexts, image outpainting, and benchmarking for image compression. To validate one of these potential utilities, we conduct a performance evaluation of different lossless image compressed formats using our 100MP images. Compared to small images for which program startup time accounts significantly during testing, time consumption on large images can better reflect the true performance of the codecs. Detailed experimental setup and results are provided in Sec. H.

Table 4 Ablation on image caption quality.

Method	Caption	FID ↓	FID <sub>patch</sub> ↓	Aesthetics ↑	GLCM Score ↑
UltraFlux	Short	126.316	55.732	6.058	1.008
	Long	<b>121.337</b>	<b>49.902</b>	<b>6.068</b>	<b>1.037</b>
Diffusion-4K	Short	142.628	90.728	5.748	0.606
	Long	<b>134.702</b>	<b>78.323</b>	<b>5.848</b>	<b>0.668</b>
FLUX.2-I (Full)	Short	135.837	51.173	5.793	0.893
	Long	<b>128.897</b>	<b>45.204</b>	<b>5.804</b>	<b>0.987</b>

## 5 Conclusion

In this paper, we present a comprehensive framework to explore the frontier of native 100MP T2I generation, encompassing data, training, and evaluation. To address key challenges in data scarcity and semantic

granularity, we introduce PixVerve-95K, a high-quality, open-source 100MP T2I dataset curated with a five-stage automated pipeline which ensures data excellence. Based on PixVerve-95K, we explore distinct training schemes to extend current T2I foundation models to native 100MP generation. Finally, our proposed PixVerve-Bench tailored for UHR scenarios further provides reliable feedback for model evaluation and selection.

**Limitations and broader impact.** As a work primarily contributing a novel dataset and evaluation benchmark, there remains significant scope for investigating UHR-specific architectural adaptations and more efficient, robust training recipes. And compared to existing general-purpose T2I datasets, the corpus size of PixVerve-95K remains still limited, though our highly scalable curation process. Considering broader impacts, while photorealistic UHR image generation greatly empowers real-world applications, the extreme realism poses heightened ethical risks concerning the proliferation of misinformation and the misuse of AI-generated content. We emphasize vigilance regarding these societal implications within the research community and advocate for multi-dimensional regulations and technical response solutions.

## References

- [1] Shuai Bai, Yuxuan Cai, Ruizhe Chen, Keqin Chen, Xionghui Chen, Zesen Cheng, Lianghao Deng, Wei Ding, Chang Gao, Chunjiang Ge, et al. Qwen3-vl technical report. *arXiv preprint arXiv:2511.21631*, 2025. 6, 7
- [2] James Betker, Gabriel Goh, Li Jing, Tim Brooks, Jianfeng Wang, Linjie Li, Long Ouyang, Juntang Zhuang, Joyce Lee, Yufei Guo, et al. Improving image generation with better captions. *Computer Science*. <https://cdn.openai.com/papers/dall-e-3.pdf>, 2(3):8, 2023. 6
- [3] Jiazi Bu, Pengyang Ling, Yujie Zhou, Pan Zhang, Tong Wu, Xiaoyi Dong, Yuhang Zang, Yuhang Cao, Dahua Lin, and Jiaqi Wang. Hiflow: Training-free high-resolution image generation with flow-aligned guidance. *arXiv preprint arXiv:2504.06232*, 2025. 2, 3, 10, 11
- [4] Huanqia Cai, Sihan Cao, Ruoyi Du, Peng Gao, Steven Hoi, Zhaohui Hou, Shijie Huang, Dengyang Jiang, Xin Jin, Liangchen Li, et al. Z-image: An efficient image generation foundation model with single-stream diffusion transformer. *arXiv preprint arXiv:2511.22699*, 2025. 1
- [5] Shuo Cao, Nan Ma, Jiayang Li, Xiaohui Li, Lihao Shao, Kaiwen Zhu, Yu Zhou, Yuandong Pu, Jiarui Wu, Jiaquan Wang, et al. Artimuse: Fine-grained image aesthetics assessment with joint scoring and expert-level understanding. *arXiv preprint arXiv:2507.14533*, 2025. 5, 7
- [6] Junsong Chen, Chongjian Ge, Enze Xie, Yue Wu, Lewei Yao, Xiaozhe Ren, Zhongdao Wang, Ping Luo, Huchuan Lu, and Zhenguo Li. Pixart- $\sigma$ : Weak-to-strong training of diffusion transformer for 4k text-to-image generation. In *European Conference on Computer Vision*, pages 74–91. Springer, 2024. 3, 4, 8
- [7] Zhennan Chen, Junwei Zhu, Xu Chen, Jiangning Zhang, Xiaobin Hu, Hanzhen Zhao, Chengjie Wang, Jian Yang, and Ying Tai. Dip: Taming diffusion models in pixel space. *arXiv preprint arXiv:2511.18822*, 2025. 3, 9
- [8] Zhennan Chen, Junwei Zhu, Xu Chen, Jiangning Zhang, Jiawei Chen, Zhuoqi Zeng, Wei Zhang, Chengjie Wang, Jian Yang, and Ying Tai. L2p: Unlocking latent potential for pixel generation. *arXiv preprint arXiv:2605.12013*, 2026. 3, 9, 10, 11
- [9] Mikael Cho. Unsplash. <https://unsplash.com/images>, 2013. 4, 17
- [10] Roger N Clark. Notes on the resolution and other details of the human eye. *Clarkvision.com*, 2005. 1
- [11] Ruoyi Du, Dongliang Chang, Timothy Hospedales, Yi-Zhe Song, and Zhanyu Ma. Demofusion: Democratising high-resolution image generation with no \$. In *Proceedings of the IEEE/CVF conference on computer vision and pattern recognition*, pages 6159–6168, 2024. 2, 3, 10, 11, 19
- [12] Ruoyi Du, Dongyang Liu, Le Zhuo, Qin Qi, Hongsheng Li, Zhanyu Ma, and Peng Gao. I-max: Maximize the resolution potential of pre-trained rectified flow transformers with projected flow. 2024. 2
- [13] Patrick Esser, Sumith Kulal, Andreas Blattmann, Rahim Entezari, Jonas Müller, Harry Saini, Yam Levi, Dominik Lorenz, Axel Sauer, Frederic Boesel, et al. Scaling rectified flow transformers for high-resolution image synthesis. In *Forty-first international conference on machine learning*, 2024. 3

- [14] Yushun Fang, Yuxiang Chen, Shibo Yin, Qiang Hu, Jiangchao Yao, Ya Zhang, Xiaoyun Zhang, and Yanfeng Wang. One-step diffusion transformer for controllable real-world image super-resolution. *arXiv preprint arXiv:2511.17138*, 2025. 5
- [15] Ian J Goodfellow, Jean Pouget-Abadie, Mehdi Mirza, Bing Xu, David Warde-Farley, Sherjil Ozair, Aaron Courville, and Yoshua Bengio. Generative adversarial nets. *Advances in neural information processing systems*, 27, 2014. 3
- [16] Google. Gemini. <https://gemini.google.com/>, 2025. 5
- [17] Robert M Haralick, Karthikeyan Shanmugam, and Its' Hak Dinstein. Textural features for image classification. *IEEE Transactions on systems, man, and cybernetics*, (6):610–621, 2007. 9, 19
- [18] Yingqing He, Shaoshu Yang, Haoxin Chen, Xiaodong Cun, Menghan Xia, Yong Zhang, Xintao Wang, Ran He, Qifeng Chen, and Ying Shan. Scalecrafter: Tuning-free higher-resolution visual generation with diffusion models. In *The Twelfth International Conference on Learning Representations*, 2023. 3
- [19] Jack Hessel, Ari Holtzman, Maxwell Forbes, Ronan Le Bras, and Yejin Choi. Clipscore: A reference-free evaluation metric for image captioning. In *Proceedings of the 2021 conference on empirical methods in natural language processing*, pages 7514–7528, 2021. 2, 10
- [20] Martin Heusel, Hubert Ramsauer, Thomas Unterthiner, Bernhard Nessler, and Sepp Hochreiter. Gans trained by a two time-scale update rule converge to a local nash equilibrium. *Advances in neural information processing systems*, 30, 2017. 2, 9
- [21] Jonathan Ho, Ajay Jain, and Pieter Abbeel. Denoising diffusion probabilistic models. *Advances in neural information processing systems*, 33:6840–6851, 2020. 3
- [22] Teng Hu, Jiangning Zhang, Zihan Su, and Ran Yi. Ultragen: High-resolution video generation with hierarchical attention. In *Proceedings of the AAAI Conference on Artificial Intelligence*, volume 40, pages 4923–4931, 2026. 1
- [23] Linjiang Huang, Rongyao Fang, Aiping Zhang, Guanglu Song, Si Liu, Yu Liu, and Hongsheng Li. Fouriscale: A frequency perspective on training-free high-resolution image synthesis. In *European conference on computer vision*, pages 196–212. Springer, 2024. 2, 3
- [24] Xinyu Huang, Yi-Jie Huang, Youcai Zhang, Weiwei Tian, Rui Feng, Yuejie Zhang, Yanchun Xie, Yaqian Li, and Lei Zhang. Open-set image tagging with multi-grained text supervision. In *Proceedings of the 33rd ACM International Conference on Multimedia*, pages 4117–4126, 2025. 6
- [25] Ingo, Bruno Joseph, and Daniel Frese. Pexels images. <https://www.pexels.com/images/>, 2014. 4, 17
- [26] Qing Jiang, Junan Huo, Xingyu Chen, Yuda Xiong, Zhaoyang Zeng, Yihao Chen, Tianhe Ren, Junzhi Yu, and Lei Zhang. Detect anything via next point prediction. *arXiv preprint arXiv:2510.12798*, 2025. 6
- [27] Yuval Kirstain, Adam Polyak, Uriel Singer, Shahbuland Matiana, Joe Penna, and Omer Levy. Pick-a-pic: An open dataset of user preferences for text-to-image generation. *Advances in neural information processing systems*, 36:36652–36663, 2023. 3
- [28] Black Forest Labs. Flux. <https://github.com/black-forest-labs/flux>, 2024. 3
- [29] Black Forest Labs. FLUX.2: Frontier Visual Intelligence. <https://bf.lai/blog/flux-2>, 2025. 1, 3, 8, 10, 11
- [30] LAION-AI. aesthetic-predictor. <https://github.com/LAION-AI/aesthetic-predictor>, 2022. 5, 9
- [31] Tianhong Li and Kaiming He. Back to basics: Let denoising generative models denoise. *arXiv preprint arXiv:2511.13720*, 2025. 3, 9
- [32] Bingchen Liu, Ehsan Akhgari, Alexander Visheratin, Aleks Kamko, Linmiao Xu, Shivam Shrivastava, Chase Lambert, Joao Souza, Suhail Doshi, and Daiqing Li. Playground v3: Improving text-to-image alignment with deep-fusion large language models. *arXiv preprint arXiv:2409.10695*, 2024. 3
- [33] Songhua Liu, Weihao Yu, Zhenxiong Tan, and Xinchao Wang. Linfusion: 1 gpu, 1 minute, 16k image. *arXiv preprint arXiv:2409.02097*, 2024. 10, 11
- [34] William Peebles and Saining Xie. Scalable diffusion models with transformers. In *Proceedings of the IEEE/CVF international conference on computer vision*, pages 4195–4205, 2023. 3
- [35] Dustin Podell, Zion English, Kyle Lacey, Andreas Blattmann, Tim Dockhorn, Jonas Müller, Joe Penna, and Robin Rombach. Sdxl: Improving latent diffusion models for high-resolution image synthesis. *arXiv preprint arXiv:2307.01952*, 2023. 3

- [36] Qwen Team. Qwen3.5: Towards Native Multimodal Agents. <https://qwen.ai/blog?id=qwen3.5>, February 2026. 9, 10, 20, 21
- [37] Aditya Ramesh, Mikhail Pavlov, Gabriel Goh, Scott Gray, Chelsea Voss, Alec Radford, Mark Chen, and Ilya Sutskever. Zero-shot text-to-image generation. In *International conference on machine learning*, pages 8821–8831. Pmlr, 2021. 3
- [38] Nikhila Ravi, Valentin Gabeur, Yuan-Ting Hu, Ronghang Hu, Chaitanya Ryali, Tengyu Ma, Haitham Khedr, Roman Rädle, Chloe Rolland, Laura Gustafson, et al. Sam 2: Segment anything in images and videos. *arXiv preprint arXiv:2408.00714*, 2024. 6
- [39] Jingjing Ren, Wenbo Li, Haoyu Chen, Renjing Pei, Bin Shao, Yong Guo, Long Peng, Fenglong Song, and Lei Zhu. Ultrapixel: Advancing ultra high-resolution image synthesis to new peaks. *Advances in Neural Information Processing Systems*, 37:111131–111171, 2024. 3, 10, 11
- [40] Robin Rombach, Andreas Blattmann, Dominik Lorenz, Patrick Esser, and Björn Ommer. High-resolution image synthesis with latent diffusion models. In *Proceedings of the IEEE/CVF conference on computer vision and pattern recognition*, pages 10684–10695, 2022. 3
- [41] Christoph Schuhmann, Richard Vencu, Romain Beaumont, Robert Kaczmarczyk, Clayton Mullis, Aarush Katta, Theo Coombes, Jenia Jitsev, and Aran Komatsuzaki. Laion-400m: Open dataset of clip-filtered 400 million image-text pairs. *arXiv preprint arXiv:2111.02114*, 2021. 3
- [42] Christoph Schuhmann, Romain Beaumont, Richard Vencu, Cade Gordon, Ross Wightman, Mehdi Cherti, Theo Coombes, Aarush Katta, Clayton Mullis, Mitchell Wortsman, et al. Laion-5b: An open large-scale dataset for training next generation image-text models. *Advances in neural information processing systems*, 35:25278–25294, 2022. 3
- [43] Claude Elwood Shannon. A mathematical theory of communication. *The Bell system technical journal*, 27(3): 379–423, 1948. 5, 19
- [44] Shuwei Shi, Wenbo Li, Yuechen Zhang, Jingwen He, Biao Gong, and Yinqiang Zheng. Resmaster: Mastering high-resolution image generation via structural and fine-grained guidance. In *Proceedings of the AAAI Conference on Artificial Intelligence*, volume 39, pages 6887–6895, 2025. 3
- [45] Chenyang Si, Ziqi Huang, Yuming Jiang, and Ziwei Liu. Freeu: Free lunch in diffusion u-net. In *Proceedings of the IEEE/CVF conference on computer vision and pattern recognition*, pages 4733–4743, 2024. 3
- [46] Luigi Sigillo, Shengfeng He, and Danilo Comminiello. Latent wavelet diffusion for ultra-high-resolution image synthesis. *arXiv preprint arXiv:2506.00433*, 2025. 3
- [47] Aaditya Singh, Adam Fry, Adam Perelman, Adam Tart, Adi Ganesh, Ahmed El-Kishky, Aidan McLaughlin, Aiden Low, AJ Ostrow, Akhila Ananthram, et al. Openai gpt-5 system card. *arXiv preprint arXiv:2601.03267*, 2025. 5
- [48] Shuai Wang, Ziteng Gao, Chenhui Zhu, Weilin Huang, and Limin Wang. Pixnerd: Pixel neural field diffusion. *arXiv preprint arXiv:2507.23268*, 2025. 3
- [49] WangXuan95. Image-compression-benchmark. <https://github.com/WangXuan95/Image-Compression-Benchmark>, 2025. 23
- [50] Chenfei Wu, Jiahao Li, Jingren Zhou, Junyang Lin, Kaiyuan Gao, Kun Yan, Sheng-ming Yin, Shuai Bai, Xiao Xu, Yilei Chen, et al. Qwen-image technical report. *arXiv preprint arXiv:2508.02324*, 2025. 3, 5, 10, 11
- [51] Chunyu Xie, Bin Wang, Fanjing Kong, Jincheng Li, Dawei Liang, Ji Ao, Dawei Leng, and Yuhui Yin. Fg-clip 2: A bilingual fine-grained vision-language alignment model. *arXiv preprint arXiv:2510.10921*, 2025. 10
- [52] Enze Xie, Junsong Chen, Junyu Chen, Han Cai, Haotian Tang, Yujun Lin, Zhekai Zhang, Muyang Li, Ligeng Zhu, Yao Lu, et al. Sana: Efficient high-resolution image synthesis with linear diffusion transformers. *arXiv preprint arXiv:2410.10629*, 2024. 1
- [53] Zhucun Xue, Jiangning Zhang, Teng Hu, Haoyang He, Yinan Chen, Yuxuan Cai, Yabiao Wang, Chengjie Wang, Yong Liu, Xiangtai Li, et al. Ultravideo: High-quality uhd video dataset with comprehensive captions. *arXiv preprint arXiv:2506.13691*, 2025. 1
- [54] An Yang, Anfeng Li, Baosong Yang, Beichen Zhang, Binyuan Hui, Bo Zheng, Bowen Yu, Chang Gao, Chengen Huang, Chenxu Lv, et al. Qwen3 technical report. *arXiv preprint arXiv:2505.09388*, 2025. 6

- [55] Tian Ye, Song Fei, and Lei Zhu. Ultraflux: Data-model co-design for high-quality native 4k text-to-image generation across diverse aspect ratios. *arXiv preprint arXiv:2511.18050*, 2025. [2](#), [3](#), [4](#), [6](#), [10](#), [11](#)
- [56] Jiangning Zhang, Teng Hu, Haoyang He, Zhucun Xue, Yabiao Wang, Chengjie Wang, Yong Liu, Xiangtai Li, and Dacheng Tao. Emov2: Pushing 5 m vision model frontier. *IEEE Transactions on Pattern Analysis and Machine Intelligence*, 2025. [8](#)
- [57] Jiangning Zhang, Junwei Zhu, Teng Hu, Yabiao Wang, Donghao Luo, Weijian Cao, Zhenye Gan, Xiaobin Hu, Zhucun Xue, and Chengjie Wang. Transform trained transformer: Accelerating naive 4k video generation over  $10\times$ . *arXiv preprint arXiv:2512.13492*, 2025. [1](#), [9](#)
- [58] Jinjin Zhang, Qiuyu Huang, Junjie Liu, Xiefan Guo, and Di Huang. Ultra-high-resolution image synthesis: Data, method and evaluation. *arXiv preprint arXiv:2506.01331*, 2025. [2](#), [3](#), [4](#), [8](#), [17](#)
- [59] Jinjin Zhang, Qiuyu Huang, Junjie Liu, Xiefan Guo, and Di Huang. Diffusion-4k: Ultra-high-resolution image synthesis with latent diffusion models. In *Proceedings of the Computer Vision and Pattern Recognition Conference*, pages 23464–23473, 2025. [2](#), [3](#), [4](#), [8](#), [10](#), [11](#)
- [60] Richard Zhang, Phillip Isola, Alexei A Efros, Eli Shechtman, and Oliver Wang. The unreasonable effectiveness of deep features as a perceptual metric. In *Proceedings of the IEEE conference on computer vision and pattern recognition*, pages 586–595, 2018. [6](#)
- [61] Chen Zhao, En Ci, Yunzhe Xu, Tiehan Fan, Shanyan Guan, Yanhao Ge, Jian Yang, and Ying Tai. Ultrahr-100k: Enhancing uhr image synthesis with a large-scale high-quality dataset. *arXiv preprint arXiv:2510.20661*, 2025. [2](#), [3](#), [4](#), [6](#), [8](#), [17](#)
- [62] Yushen Zuo, Qi Zheng, Mingyang Wu, Xinrui Jiang, Renjie Li, Jian Wang, Yide Zhang, Gengchen Mai, Lihong V Wang, James Zou, et al. 4kagent: agentic any image to 4k super-resolution. *arXiv preprint arXiv:2507.07105*, 2025. [1](#)

## Appendix

The appendix presents the following sections to strengthen the main manuscript:

- **Sec. A** provides implementation details of flatness detection.
- **Sec. B** provides a further frequency-domain analysis to confirm the quality of PixVerve-95K.
- **Sec. C** provides a detailed clarification on the licensing for our proposed dataset to ensure transparency and ethical compliance.
- **Sec. D** presents more qualitative samples in PixVerve-95K.
- **Sec. E** provides more training and inference details of different approaches.
- **Sec. F** provides additional details on metrics of PixVerve-Bench, including specific evaluation procedures, scoring formulas, and human alignment analysis.
- **Sec. G** provides more quantitative and qualitative results of model performance.
- **Sec. H** provides benchmark results of image compression using our 100MP images.
- **Sec. I** shows the prompts used for MLLM evaluation in PixVerve-Bench.

### A Implementation Details of Flatness Detection

In the stage of preliminary data purification (Sec. 3.1.2), we conduct a flatness detection procedure based on the Sobel variance. Each image in the raw data pool is first converted to grayscale and partitioned into  $240 \times 240$  non-overlapping patches. We then compute the gradient magnitude  $G_{mag} = \sqrt{G_x^2 + G_y^2}$  for each patch, using Sobel operators with a kernel size of 3. A patch is categorized as “textureless” if the variance of its gradient magnitude falls below a predefined threshold of 750, and an image is discarded if the proportion of textureless patches exceeds 97.5%. Notably, both thresholds are intentionally conservative and determined empirically through manual visual audits, which ensures the efficient elimination of overly flat images while still preserving legitimate low-texture content.

### B Further Analysis of PixVerve-95K Dataset

We conduct an extended frequency-domain quality analysis of our PixVerve-95K dataset, utilizing the Radially Averaged Power Spectrum (RAPS). This analysis intuitively presents the power distribution across spatial frequencies, providing insights into the realism of synthesized high-frequency textures. As illustrated in Fig. A1 (a), the power spectral density of our synthetic 100MP data closely matches the native distribution across the entire frequency range; notably, no significant energy attenuation is observed in the high-frequency regime, confirming the micro-texture fidelity of our rigorously preserved synthetic data. Furthermore, we analyze the consistency between down-sampled SR images and their original low-resolution (LR) counterparts. The alignment of the power spectrum shown in Fig. A1 (b) indicates that our data curation pipeline maintains global structural consistency and adheres to the underlying distribution of the original images. Overall, this analysis further substantiates that our PixVerve-95K provides high-quality, ultra-high-resolution data, ensuring its reliability for downstream large-scale generative modeling.

### C Licensing and Dataset Release

This section provides a detailed account of the licensing for our proposed dataset. As illustrated in the main manuscript, a significant portion of the images was sourced from Pexels [25] and Unsplash [9]. These platforms operate under permissive licenses that grant broad permissions for downloading, using, and modifying visual content for both commercial and non-commercial purposes without financial obligation. Additionally, a subset is from Aesthetic-Train-V2 [58] and UltraHR-100K [61], which are governed by the MIT License and the Creative Commons Attribution-NonCommercial 4.0 (CC BY-NC 4.0) License, respectively. Both frameworks

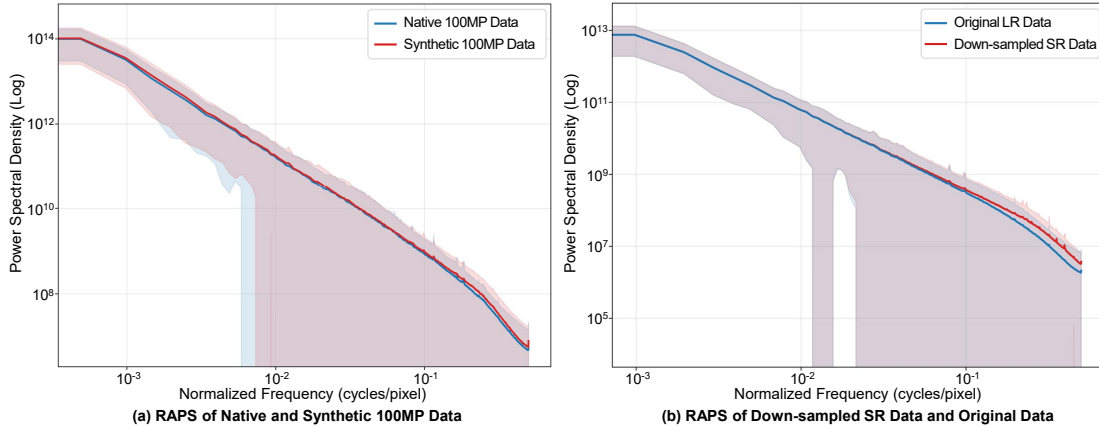


Figure A1 RAPS comparisons.

permit the utilization of data for non-commercial research purposes. Therefore, we affirm that our dataset is in full compliance with current copyright laws and privacy regulations, and this dataset is released under the CC BY-NC 4.0 license to prevent unauthorized commercial exploitation.

## D Qualitative Samples in PixVerve-95K Dataset

Fig. A5 and Fig. A6 show two qualitative samples in our PixVerve-95K dataset. Best viewed zoomed-in.

## E More Training and Inference Details

### E.1 Training Details

For each training scheme, we report the fine-tuning epochs at each resolution scale and the corresponding NVIDIA H20 GPU hours in Tab. A1. GPU hours are computed as the product of the number of NVIDIA H20 GPUs used and the wall-clock training time. Certain schemes do not complete the full three-stage training process since they have exhibited unsatisfactory performance at low resolutions. These computational details are provided to ensure the reproducibility of our main experimental results.

For *Scheme I*, we consider both full-parameter fine-tuning and LoRA for parameter-efficient fine-tuning. Specifically, the full-parameter trained 8K model is initialized from the 4K checkpoint trained for 3 epochs, and is further fine-tuned for 0.25 epochs at 8K resolution. All LoRA models at different resolutions are independently fine-tuned from the same base model, FLUX.2-klein-base-4B, rather than being initialized from lower-resolution LoRA checkpoints. For *Scheme II*, we report the cost of full-parameter fine-tuning with window-attention retrofitting at 4K resolution. For *Scheme III*, the training also follows a progressive curriculum: the 8K model is initialized from the 4K checkpoint, while the 10K model is initialized from the 8K checkpoint after 1 epoch of training.

Table A1 Training details of different schemes.

Training Resolution	Number of Epochs	Total H20 GPU Hours
<b>Scheme I (Full)</b>		
4K	6	21,888
8K	0.25	10,752
<b>Scheme I (LoRA)</b>		
4K	3	10,368
8K	0.25	10,752
10K	0.32	28,416
<b>Scheme II</b>		
4K	3	9,216
<b>Scheme III</b>		
4K	4.3	8,448
8K	2.9	18,432
10K	1.7	23,040

### E.2 Inference Details

In this section, we report the per-sample inference cost of different methods in Tab. A2. The number of GPUs denotes the number of devices jointly used to generate one sample, rather than the batch size, and the inference time is measured as wall-clock latency in seconds.

For *Scheme I*, as we expect, full fine-tuning and LoRA fine-tuning show nearly identical inference latency, since LoRA changes the adaptation parameterization but does not alter the dominant full-attention computation over the high-resolution latent grid. Therefore, the latency of both variants grows rapidly as the inference resolution increases. Increasing the resolution from 4K to 8K raises the inference time from 103s to over 1,200s, and the LoRA variant requires nearly 3,000s at 10K. Moreover, all these runs require 8 GPUs for generating a single sample, revealing the substantial memory and deployment cost of full-attention latent diffusion at the 100MP scale.

*Scheme II* reduces the 4K inference time from 103s to 71s under the same 8-GPU setting, which verifies that the window-attention retrofitting effectively lowers the attention cost while retaining compatibility with the pretrained latent diffusion backbone. However, it still inherits the multi-GPU inference requirement of the latent-space pipeline, making it an efficiency improvement rather than a complete solution to the deployment bottleneck.

In contrast, *Scheme III* exhibits the most favorable inference behavior. It runs on a single GPU card at all evaluated resolutions, with inference times of 58s, 70s, and 88s at 4K, 8K, and 10K, respectively. The nearly flat latency derives from the adaptive patch-size design, which controls the transformer sequence length as the image resolution increases. Compared to the representative training-free method, DemoFusion, *Scheme III* is 16.3 $\times$ , 90.9 $\times$ , and 155.6 $\times$  faster at 4K, 8K, and 10K, respectively.

Overall, these results reveal a clear efficiency and deployability trade-off. Full-attention LDM fine-tuning preserves the original computation of the foundation model but becomes prohibitively expensive at ultra-high resolutions. Window-attention retrofitting provides a useful intermediate point by reducing latent attention cost. Patch-based pixel diffusion, although relying on coarser patch-level representations at higher resolutions, is the only explored scheme that enables native 100MP image generation with a single GPU card and sub-minute latency.

## F Additional Details on Metrics of PixVerve-Bench

### F.1 GLCM Score

In this section, we provide the detailed computation procedure of the GLCM Score, which is introduced to quantitatively evaluate the texture granularity in PixVerve-Bench. The GLCM Score is computed by first quantizing the grayscale intensities of the generated image into 64 levels and partitioning it into a set of  $64 \times 64$  non-overlapping local patches  $\{p_1, p_2, \dots, p_P\}$ . For each patch  $p_i$ , a normalized Gray Level Co-occurrence Matrix [17]  $G_{p_i}$  is constructed across multiple predefined distances  $\delta \in \{1, 2, 3, 4\}$  and orientations  $\theta \in \{0, \frac{\pi}{4}, \frac{\pi}{2}, \frac{3\pi}{4}\}$  to capture spatial correlations. Subsequently, the detail richness of  $p_i$  is measured via the average Shannon entropy [43], which is calculated over all spatial parameters and denoted as  $H(G_{p_i})$ . Finally, the GLCM Score  $S$  for the entire image is defined as the arithmetic mean of the entropy values across all  $P$

**Table A2** Inference details of different methods.

Inference Resolution	Number of GPUs	Inference time (s)
<b><i>Scheme I (Full)</i></b>		
4K	8	103
8K	8	1,234
<b><i>Scheme I (LoRA)</i></b>		
4K	8	103
8K	8	1,252
10K	8	2,977
<b><i>Scheme II</i></b>		
4K	8	71
<b><i>Scheme III</i></b>		
4K	1	58
8K	1	70
10K	1	88
<b>DemoFusion [11]</b>		
4K	1	945
8K	1	6,366
10K	1	13,689

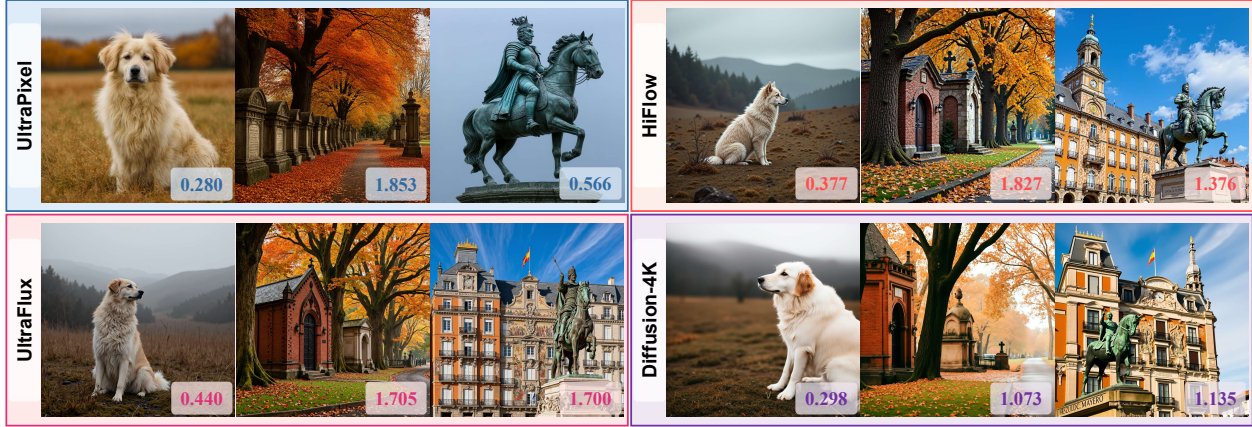


**Figure A2 Case visualization of the GLCM Score.** We present representative  $4096 \times 4096$  images generated by UltraPixel, HiFlow, UltraFlux, and Diffusion-4K along with their corresponding scores, demonstrating that higher scores indicate richer texture. Prompts are from PixVerve-Bench.

patches:

$$S = \frac{1}{P} \sum_{i=1}^P H(G_{p_i}),$$

providing an objective statistical assessment of the micro-structural complexity which is essential for UHR image generation. The case visualization of the GLCM Score is shown in Fig. A2.

## F.2 Multi-scale Fidelity Index (MSFI)

In this section, we provide the detailed procedure and formulas of computing the Multi-scale Fidelity Index (MSFI).

**Taxonomy of evaluation dimensions.** As described in the main manuscript, the MSFI systematically assesses UHR image fidelity across two complementary dimensions, spanning nine fine-grained sub-dimensions that each target a distinct artifact category. Tab. A3 summarizes the evaluation dimensions, sub-dimensions, corresponding descriptions, and criteria.

**Detailed evaluation procedures.** For each predefined sub-dimension, we instruct Qwen3.5-35B-A3B [36] to assign a score on a five-point scale reflecting artifact severity. Specifically, for global-scale assessment, the MLLM evaluates the complete generated image resized to a standardized resolution. For local-scale assessment, we adopt the hybrid strategy used in Sec. 3.1.4 to sample ten representative local patches per image, with the patch size set to  $512 \times 512$  for images below 8K resolution and  $1024 \times 1024$  otherwise; during each scoring round, the target local patch is evaluated at its native resolution, with the down-sampled complete image provided for contextual reference and the patch’s relative spatial coordinates explicitly specified in the prompt; finally, the local-scale fidelity score of each image is derived by averaging the ratings assigned to the ten sampled patches. Furthermore, we provide detailed definitions for each sub-dimension and descriptions for each score level to ensure that the model maintains consistent criteria across multiple rounds of evaluations. The case visualization of each sub-dimension is shown in Fig. A3. The prompts used for global-scale and local-scale fidelity evaluation are provided in Sec. I.

**Unified scoring formulation.** For a given evaluation dimension  $D$  (global-scale or local-scale), let the set of scores for different sub-dimensions be  $\{s_1, s_2, \dots, s_{n_D}\}$  with corresponding weights  $\{w_1, w_2, \dots, w_{n_D}\}$ . The score for dimension  $D$  is defined as:

$$S_D = \frac{\sum_{i=1}^{n_D} w_i \cdot s_i}{\sum_{i=1}^{n_D} w_i}.$$

The weights are determined through a user study, where participants provided importance ratings (1-5) for all sub-dimensions. These ratings were averaged, rounded to the nearest integer, and applied directly as the

**Table A3 Description and evaluation criteria for each sub-dimension of the MSFI.** We detail the hierarchical framework designed to assess the fidelity of UHR images across dual scales.

Dimension	Sub-dimension	Description and Evaluation Criteria
<b>Global-scale</b>	Structural Coherence	Evaluates the physical plausibility of overall spatial arrangements and global geometric integrity of entities, ensuring anatomical correctness ( <i>e.g.</i> , no missing or redundant limbs).
	Perspective Integrity	Assesses whether vanishing points and the relative scale of objects at varying depths conform to perspective principles, identifying any geometric distortions against common sense.
	Lighting Consistency	Inspects global illumination for naturalism, checking for consistent light direction and the absence of artificial luminance gradients or disjointed shading.
	Color Harmony	Examines chromatic transitions for smoothness, checking for quantization artifacts ( <i>e.g.</i> , color banding) or unnatural boundary blurring between distinct color blocks.
<b>Local-scale</b>	Noise & Grain Existence	Detects stochastic high-frequency chroma noise and unnatural graininess within local patches that deviate from the expected sensor behavior.
	Generative Artifacts	Scrutinizes local patches for typical synthesis flaws, including checkerboard patterns, aliasing, and edge halos.
	Texture Fidelity	Differentiates between realistic surface roughness and “plastic-like” oversmoothing, ensuring natural materials exhibit stochastic randomness rather than mechanical repetition.
	Micro-geometry Coherence	Analyzes the continuity of local contours at the pixel level, penalizing unacceptable jitter, “staircase” effects, or jagged edges in high-contrast regions.
	Sharpness Consistency	Validates the consistency of the focal plane, ensuring that areas within the same depth of field maintain uniform clarity without abnormal, localized blurring.

weights. The overall MSFI for image  $I$  is given by:

$$\text{MSFI}(I) = S_{\text{global}}(I) + w_l \cdot \frac{1}{10} \sum_{i=1}^{10} S_{\text{local}}(I, i),$$

where  $S_{\text{global}}(I)$  and  $S_{\text{local}}(I, i)$  denote the aggregated global fidelity score of  $I$  and the local fidelity score of the  $i^{\text{th}}$  patch sampled from  $I$ . Notably, we set the weighting factor  $w_l$  as  $\frac{S_{\text{global}}(I)}{5}$ , claiming that global structural integrity is a fundamental prerequisite for microscopic realism. This formulation effectively penalizes “structurally incoherent” images that might otherwise attain misleadingly high scores due to sharp local textures. Consequently, the MSFI ranges from 1.2 to 10, where a score approaching 10 signifies superior multi-scale fidelity.

### F.3 Instance-centric Compliance Score (ICS)

In this section, we provide the specific evaluation procedure and scoring formulas of the Instance-centric Compliance Score (ICS), which is proposed to quantify how precisely visual instances adhere to complex textual descriptions. We implement the ICS evaluator leveraging the Qwen3.5-35B-A3B model [36].

**Evaluation dimensions.** The assessment of the ICS is performed across three distinct dimensions, each scored by MLLM on a ten-point scale based on specific rubrics:

- **Instance Existence Verification (IEV):** This dimension serves as the gatekeeper, identifying whether all primary and secondary instances specified in the long caption are present. It focuses purely on presence or absence rather than quality.

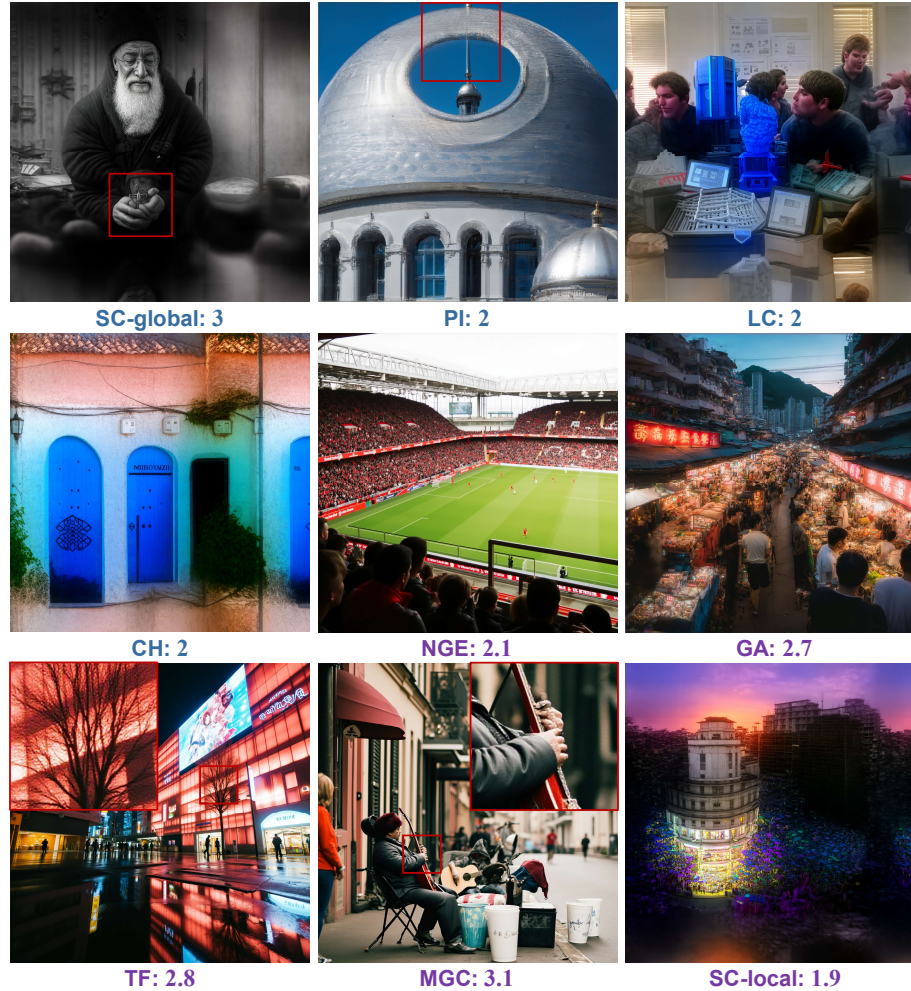


**Figure A3 Case visualization of the MSFI.** We present typical examples of low-quality generations across the nine sub-dimensions, accompanied by their corresponding scores. **Blue scores** denote sub-dimension ratings for global-scale fidelity, while **purple scores** indicate those for local-scale fidelity, which are the arithmetic means of scores across ten sampled patches. SC-global, PI, LC, CH, NGE, GA, TF, MGC, and SC-local denote the nine MLLM-as-a-judge sub-dimensions described in Tab. A3, respectively. Red bounding boxes are utilized to highlight specific degradations identified within the examples.

- **Appearance Attribute Alignment (AAA):** For identified instances, this dimension evaluates whether the corresponding visual attributes (*e.g.*, color, texture, material, shape, *etc.*) are compliant with the textual description.
- **Spatial Relation Accuracy (SRA):** This dimension assesses whether the relative positioning (*e.g.*, “left of”, “behind”, “in the foreground”, *etc.*) and the logical perspective are accurately depicted in the synthesized images.

We also provide detailed descriptions for each score level to ensure consistent criteria across multiple rounds of evaluations. The prompt used for instance-centric compliance evaluation is provided in Sec. I.

**Unified scoring formulation.** For each generated image, we instruct the MLLM to evaluate the aforementioned three dimensions, yielding a set of raw scores denoted as  $\{S_{IEV}, S_{AAA}, S_{SRA}\}$ . Considering the hierarchical dependency where appearance attributes and spatial relations are contingent upon the existence of the instances themselves, we employ a gated weighted average strategy to synthesize these three-dimensional

scores into the final ICS:

$$\text{ICS} = \sqrt{\frac{S_{IEV}}{10}} \times (\alpha \cdot S_{AAA} + \beta \cdot S_{SRA}),$$

where the term  $\sqrt{S_{IEV}/10}$  acts as a penalty for instance omissions. In our implementation, we set  $\alpha = 0.6$  and  $\beta = 0.4$  to prioritize appearance attribute fidelity. Consequently, an ICS nearing 10 indicates superior instance-centric compliance, while a low score reflects either obvious entity omissions or a misalignment of visual details.

## F.4 Human Alignment for Metric Validation

To validate that our proposed automated MSFI and ICS align with human-centric preferences, this section provides a quantitative analysis. We select four representative text-to-image models,  $\mathcal{M} = \{M_A, M_B, M_C, M_D\}$ , to generate 4K and 8K images. For each resolution, 30 unique prompts are utilized, resulting in a total of  $C_4^2 \times 60 = 360$  pair-wise comparison sets. We recruit 8 participants to conduct this human preference study, each tasked with evaluating 90 image pairs to ensure that every pair receives two independent annotations. Participants are provided with detailed definitions and illustrative examples for two evaluation dimensions: *Image Fidelity* and *Instance-centric Semantic Alignment*, which correspond to the MSFI and ICS, respectively. For each comparison pair  $(I_i, I_j)$  generated by  $M_i$  and  $M_j$ , annotators are instructed to indicate a preference or label the pair as “indistinguishable”. Let  $s_{i,j}$  be the score assigned to model  $M_i$  in a single comparison:

$$s_{i,j} = \begin{cases} 1.0 & \text{if } M_i \text{ is preferred,} \\ 0.5 & \text{if indistinguishable,} \\ 0 & \text{if } M_j \text{ is preferred.} \end{cases}$$

For each evaluation dimension, the final human preference score for each model is computed as the total score divided by the number of comparisons. We observe that the performance rankings of the four models yielded by our proposed MSFI and ICS perfectly match the rankings derived from human preference scores. This consistency demonstrates that the MSFI and ICS are well-aligned with human subjective judgments in distinguishing the quality and alignment capabilities of different T2I models.

## G More Quantitative and Qualitative Results

### G.1 More Quantitative Results

Tab. A4 details the performance of different methods on the MSFI. SC-global, PI, LC, CH, NGE, GA, TF, MGC, and SC-local denote the nine MLLM-as-a-judge sub-dimensions described in Tab. A3, respectively.

### G.2 More Qualitative Results

Fig. A4 visualizes the qualitative comparison of 4K image generations under short and long prompting settings. All case pairs are generated by our FLUX.2-I (Full).

## H Benchmarking for Image Compression at 100MP Scale

Following the benchmark specifications in [49], we convert 25 images from our dataset into PNM format (a simple image format which stores raw pixels) for standard testing. A total of 20 image compressed formats are evaluated under strict lossless settings. The testing environment consists of a 12<sup>th</sup> Gen Intel i7-12700H CPU @2.30 GHz, 16 GB of RAM, and the Windows 11 operating system, and all codecs run in a single thread. The detailed benchmark results, including compressed size, compression time, and decompression time, are summarized in Tab. A5.

**Table A4 Detailed MSFI comparison across various UHR scales, dimensions, and sub-dimensions.** – indicates complete failures such as producing meaningless textures or black images, which are not applicable to the semantics-agnostic MSFI. Higher values indicate better performance.

Resolution (height × width)	Method	Dimension Performance		Sub-dimension Performance								
		Global Fidelity	Local Fidelity	SC-global	PI	LC	CH	NGE	GA	TF	MGC	SC-local
<b>4K</b> (4096 × 4096)	FLUX.2-klein-base-4B	3.955	4.366	3.485	4.260	4.240	4.385	4.326	4.381	4.332	4.409	4.426
	Qwen-Image	4.343	4.547	4.010	4.470	4.620	4.710	4.546	4.560	4.515	4.573	4.583
	L2P	4.572	2.539	4.255	4.820	4.785	4.780	2.508	2.550	2.531	2.556	2.556
	DemoFusion	4.237	4.731	3.685	4.510	4.665	4.780	4.786	4.713	4.704	4.724	4.776
	LinFusion	4.410	4.264	3.935	4.685	4.750	4.845	4.315	4.291	4.202	4.295	4.301
	HiFlow	4.471	4.848	4.180	4.910	4.915	4.930	4.889	4.831	4.828	4.847	4.885
	UltraPixel	4.688	4.761	4.315	4.945	4.950	4.975	4.783	4.762	4.741	4.766	4.786
	UltraFlux	4.669	4.330	4.260	4.945	4.965	4.980	4.314	4.341	4.312	4.354	4.351
	Diffusion-4K	4.577	4.151	4.165	4.860	4.875	4.885	4.125	4.171	4.121	4.186	4.187
	FLUX.2-I (Full)	4.561	4.762	4.120	4.860	4.870	4.905	4.760	4.765	4.747	4.770	4.786
	FLUX.2-I (LoRA)	4.575	4.801	4.155	4.865	4.855	4.910	4.815	4.796	4.785	4.807	4.830
	FLUX.2-II	4.150	4.784	3.650	4.530	4.365	4.615	4.791	4.792	4.761	4.797	4.814
L2P-III	4.493	2.764	4.165	4.815	4.660	4.665	2.750	2.768	2.753	2.782	2.785	
<b>8K</b> (8192 × 8192)	FLUX.2-klein-base-4B	–	–	–	–	–	–	–	–	–	–	–
	L2P	4.558	3.317	4.240	4.830	4.735	4.770	3.216	3.361	3.292	3.377	3.358
	DemoFusion	3.647	4.550	3.075	3.770	4.110	4.430	4.763	4.615	4.313	4.647	4.735
	LinFusion	4.250	4.173	3.755	4.510	4.615	4.730	4.230	4.193	4.121	4.193	4.200
	FLUX.2-I (Full)	–	–	–	–	–	–	–	–	–	–	–
	FLUX.2-I (LoRA)	–	–	–	–	–	–	–	–	–	–	–
L2P-III	3.490	2.580	3.255	4.020	3.410	3.365	2.542	2.594	2.563	2.601	2.618	
<b>10K</b> (10240 × 10240)	L2P	4.301	3.573	3.970	4.585	4.495	4.510	3.468	3.617	3.548	3.627	3.627
	DemoFusion	3.448	4.730	2.890	3.525	3.945	4.230	4.810	4.704	4.697	4.722	4.785
	LinFusion	4.139	4.090	3.620	4.400	4.545	4.640	4.145	4.113	4.041	4.107	4.108
	L2P-III	3.577	2.746	3.204	4.017	3.744	3.680	2.711	2.745	2.721	2.757	2.835



**Figure A4 Qualitative comparison of 4K image generations under short and long prompting settings.** *Top:* images generated by our FLUX.2-I (Full) using short captions; *bottom:* generated images using corresponding long captions.

**Table A5** Performance comparison of different lossless image compressed formats at the 100MP scale.

Compressed Format	Compressed Size (bytes) ↓	Compression Time (s) ↓	Decompression Time (s) ↓
fNBLI	2152173140	68.343	44.276
NBLI (-g)	2122763920	483.106	429.641
HALIC	2327457195	23.266	33.072
HALICfast	2501106140	16.154	25.109
KVICK	2467300114	60.579	43.413
QIC	2675297097	32.500	30.960
QLIC2	2415123224	40.452	38.795
LEA	1898470283	772.283	870.666
BMF	2260500400	554.801	254.198
BIM	2399426455	301.153	339.631
QOI	3685837372	28.764	22.864
QOIR	3421495512	28.557	26.181
ZPNG	3003246621	36.658	29.638
PNG (optimizing=False)	3207101968	760.569	65.350
PNG (optimizing=True)	3138083188	5417.594	74.167
JPEG-XL (-q 100 -e 1)	2765116877	77.526	107.456
JPEG-XL (-q 100 -e 2)	2557728595	233.997	112.632
JPEG-XL (-q 100 -e 3)	2315011289	511.114	314.402
WEBP (lossless m1)	2387603822	2536.114	75.605
JPEG-LS	2969890552	234.688	199.415

## I Prompts for MLLM Evaluation

### Global-scale Fidelity Evaluation Prompt

#### # ROLE AND TASK FORMULATION:

You are a professional image quality assessment (IQA) and scoring expert specializing in T2I evaluation. Your task is to carefully evaluate the **global-scale fidelity** of the provided synthetic image across 4 dimensions. Please focus on the overall composition and structure, geometric and physical logic, and macro-scale consistency.

#### # CRITICAL SCORING RULES (Must Strictly Follow):

- Objectivity & Fairness:** Maintain an objective stance throughout the evaluation process and base your judgement on visual evidence with the same standard instead of subjective preference.
- Focus Solely on Fidelity:** Consider the image category and expected characteristics while avoiding any bias towards the content of the image. Score based on the visual quality and fidelity aspects solely.
- Independence:** Evaluate each dimension independently without any halo effects.
- Rigor:** Apply strict criteria and any noticeable artifact should be reflected in the scoring. Maintain a high standard for what constitutes a “5” (Excellent).

#### # EVALUATION RUBRICS:

##### ## 1. Structural Coherence (SC-global)

Check whether the geometric structure of the entities is correct, whether there are any missing or redundant limbs, and whether the overall spatial relations are consistent with physical common sense.

- 5 (Excellent): Flawless physical logic. Objects are perfectly formed; no missing/extra parts.
- 4 (Good): Minor structural oddities that don't distract from the main subject.
- 3 (Fair): Noticeable structural errors (e.g., slightly deformed limbs or merged background objects).
- 2 (Poor): Obvious physical failures; objects are partially collapsed or mutated.
- 1 (Very Poor): Severe structural collapse; chaotic composition; unrecognizable forms.

##### ## 2. Perspective Integrity (PI)

Check whether the perspective relationship between objects at different distances conforms to the principles of perspective, and whether there is any distorted perspective.

- 5 (Excellent): Flawless perspective and geometric projection. Vanishing points and horizon lines align accurately.
- 4 (Good): Slight perspective tilt, but geometric projection still feels natural.
- 3 (Fair): Distorted depth; objects at different distances feel “stacked” or misaligned.

- 2 (Poor): Severe geometric warping; architectural lines curve unnaturally or conflict.
- 1 (Very Poor): Multiple conflicting vanishing points or warped architectural lines; total perspective failure.

### ### 3. Lighting Consistency (LC)

Check whether the overall lighting has consistency with that of a natural image, and whether there are obviously artificial brightness gradients.

- 5 (Excellent): Unified light source. Shadows, highlights, and reflections follow ray-tracing logic.
- 4 (Good): Consistent lighting, but subtle mismatch in shadow softness or intensity.
- 3 (Fair): Ambiguous light source. Some objects appear “self-lit” without casting shadows.
- 2 (Poor): Contradictory lighting directions. Shadows cast in different ways for nearby objects.
- 1 (Very Poor): Complete lighting failure; flat “sticker-like” objects with zero interaction with the environment.

### ### 4. Color Harmony (CH)

Check whether the overall color transitions are smooth and natural, and whether there are issues such as blurred edges of color blocks and color banding.

- 5 (Excellent): Natural color gamut. Smooth gradients; no banding or abnormal color noise.
- 4 (Good): High-quality color, though slight over-saturation or other issues in small areas.
- 3 (Fair): Visible color banding in gradients. Slight chromatic aberrations.
- 2 (Poor): Patchy color blocks; unnatural “neon” artifacts or gray/dull patches in vibrant areas.
- 1 (Very Poor): Severe color corruption; massive chromatic noise or broken color channels.

#### # OUTPUT RULES (Must Strictly Follow):

1. You MUST follow a strict 5-point scale and provide a score as an **INTEGER** from 1 to 5 only for each dimension.
2. Provide the final output strictly **in a JSON object inside the <json> tag**.
3. The <json> block MUST contain **ONLY** the valid JSON object. No markdown code blocks or extra text.
4. Keys: “SC-global”, “PI”, “LC”, “CH” represent the scores for the 4 dimensions respectively, and “reasoning” is a concise explanation justifying the scores. Ensure the JSON property names are enclosed in double quotes and there are no trailing commas in the JSON object.

#### # OUTPUT FORMAT:

```
<json>
{
  "SC-global": int,
  "PI": int,
  "LC": int,
  "CH": int,
  "reasoning": "A concise explanation justifying the four-dimensional scores."
}
</json>
```

Now, please evaluate the **global-scale fidelity** of the provided image based on the above criteria and output the scores and reasoning in the specified **JSON** format.

## Local-scale Fidelity Evaluation Prompt

#### # ROLE AND TASK FORMULATION:

You are a professional image quality assessment (IQA) and scoring expert specializing in local fine-grained details evaluation. Your task is to carefully evaluate the **local-scale fidelity** of the provided **local patch** of an ultra-high-resolution synthetic image across 5 dimensions. To ensure high-quality evaluation, please adhere to the following guidelines:

#### # IMPORTANT CONTEXT:

- **Image 1 (First):** This is the **LOCAL PATCH** (target for scoring). Ignore incomplete objects or composition issues. Focus only on the visual quality of the visible area.
- **Image 2 (Second):** This is the **FULL GLOBAL IMAGE** (for contextual reference). **DO NOT** use this image for direct visual analysis or evaluation. Use this image **ONLY** for **understanding the original image’s theme and global context**.
- **Patch Location:** The local patch (Image 1) corresponds to the area defined by the relative coordinates `{relative_coords}` in the global image (Image 2). The relative coordinates are normalized  $[x_{min}, y_{min}, x_{max}, y_{max}]$ , where  $[0,0]$  is the top-left corner and  $[1,1]$  is the bottom-right corner of the global image.

#### # CRITICAL SCORING RULES (Must Strictly Follow):

1. **Objectivity & Fairness:** Maintain an objective stance throughout the evaluation process and base your judgement on visual evidence with the same standard instead of subjective preference.
2. **Focus Solely on Fidelity:** Consider the image category and expected characteristics while avoiding any bias towards the content of the image. Score based on the visual quality and fidelity aspects solely.
3. **Local-to-Global Evaluation:** Evaluate the details in Image 1, and use Image 2 to distinguish between “intended bokeh/blur” and “accidental artifacts”.

4. **\*\*Coordinates Reference:\*\*** Use the rectangular bounding box only to understand the local patch's location in the overall image context, but DO NOT directly compare the local patch to the global image for pixel-level details.
5. **\*\*Independence:\*\*** Evaluate each dimension independently without any halo effects.
6. **\*\*Rigor:\*\*** Apply strict criteria and any noticeable artifact should be reflected in the scoring. Maintain a high standard for what constitutes a "5" (Excellent).

#### # EVALUATION RUBRICS:

Please evaluate the microscopic details and fidelity of the **\*\*Local Patch (Image 1)\*\*** across the 5 dimensions below, while using the Global Image (Image 2) and the relative coordinates `{relative_coords}` as reference.

##### ### 1. Noise and Grain Existence (NGE)

Check whether there is random high-frequency color noise and obvious color graininess in the local patch.

- 5 (Excellent): Crystal clean and realistic cinematic grain. Zero digital noise or compression blocks. Grain looks like natural film if present.
- 4 (Good): Slight luminance noise, barely visible at 100% zoom.
- 3 (Fair): Noticeable noise or grain that distracts from the details, especially in shadow areas.
- 2 (Poor): Heavy salt-and-pepper noise or distracting grain.
- 1 (Very Poor): Image details are buried under severe noise or compression corruption.

##### ### 2. Generative Artifacts (GA)

- 5 (Excellent): No AI-specific artifacts. Details look photo-realistic and like they were captured by a high-end CMOS sensor.
- 4 (Good): Minor generative patterns that require close inspection to find.
- 3 (Fair): Noticeable AI "melting" or "waxy" textures where details should be sharp.
- 2 (Poor): Hallucinated textures or "ghosting" artifacts typical of diffusion models.
- 1 (Very Poor): Massive generative collapse; "AI-soup" textures.

##### ### 3. Texture Fidelity (TF)

Check whether the local patch presents plastic-like oversmoothing, and for natural objects such as wood and fabric, whether the texture has randomness rather than mechanical repetition.

- 5 (Excellent): Tactile realism. Skin pores, fabric weaves, or surface grit are ultra-sharp and authentic.
- 4 (Good): High detail, but slightly "soft" or over-regularized texture.
- 3 (Fair): Texture is visible but "flat"; lacks the micro-depth of real-world surfaces.
- 2 (Poor): Over-smoothed "plastic" look; details are smeared out.
- 1 (Very Poor): Completely blurred or "mushy" surfaces with zero recognizable texture.

##### ### 4. Micro-geometry Coherence (MGC)

Check at a local scale whether the lines show unacceptable jitter or jagged edges.

- 5 (Excellent): Perfect edge continuity. Fine lines (e.g., hair, wires) are smooth at the pixel level.
- 4 (Good): Sharp edges, though very minor aliasing (stair-stepping) visible on diagonals.
- 3 (Fair): Jagged edges or slight shimmering; fine lines appear broken in some places.
- 2 (Poor): Severe aliasing; pixelated edges; micro-structures look "broken".
- 1 (Very Poor): Total geometric chaos at the micro-level; edges are unrecognizable.

##### ### 5. Sharpness Consistency (SC-local)

Check whether there are unnatural blurry patches (i.e., within the same focal plane some areas is clear enough while others are abnormally blurry).

- 5 (Excellent): Natural optical sharpness variation consistent with depth of field. No inconsistent blur patches within the same focal plane.
- 4 (Good): Slightly soft, but no inconsistent blur patches within the same focal plane.
- 3 (Fair): Noticeable inconsistency in sharpness; some areas look artificially sharpened while others are blurry without a natural depth-of-field reason.
- 2 (Poor): Obvious sharpness inconsistency; "cut-and-paste" feel where the patch looks like it was taken from a different image with different focus.
- 1 (Very Poor): Severe sharpness failure; the patch looks like a low-quality thumbnail pasted into the global image.

#### # OUTPUT RULES (Must Strictly Follow):

1. You **MUST** follow a strict 5-point scale and provide a score as an **\*\*INTEGER from 1 to 5 only\*\*** for each dimension.
2. Provide the final output strictly **\*\*in a JSON object inside the `<json>` tag\*\***.
3. The `<json>` block **MUST** contain **ONLY** the valid JSON object. No markdown code blocks or extra text.
4. Keys: "NGE", "GA", "TF", "MGC", "SC-local" represent the scores for the 5 dimensions respectively, and "reasoning" is a concise explanation justifying the scores. Ensure the JSON property names are enclosed in double quotes and there are no trailing commas in the JSON object.

#### # OUTPUT FORMAT:

```
<json>
{{
  "NGE": int,
  "GA": int,
  "TF": int,
  "MGC": int,
```

```

    "SC-local": int,
    "reasoning": "A concise explanation justifying the five-dimensional scores."
  }}
</json>

```

Now, please evaluate the **local-scale fidelity** of the provided local crop based on the above criteria and output the scores and reasoning in the specified **JSON** format.

### Instance-centric Compliance Evaluation Prompt

#### # ROLE AND TASK FORMULATION:

You are a professional image quality assessment and scoring expert specializing in Text-to-Image (T2I) semantic alignment evaluation. Your task is to carefully perform a fine-grained, instance-centric assessment of the provided synthesized image based on its initial detailed long caption.

**Input Long Caption:** "{long\_caption}"

#### # METRIC DIMENSIONS AND BOUNDARIES:

Please evaluate the image across the following three distinct, hierarchical dimensions, strictly adhering to the defined criteria and boundaries:

- IEV (Instance Existence Verification):** Inspect whether all instances explicitly mentioned in the long caption are present. Focus strictly and solely on presence or absence rather than quality.
- AAA (Appearance Attribute Alignment):** For each instance that exists, assess whether its visual attributes (color, texture, material, size, shape) align with the description in the long caption. This requires detailed cross-referencing between the caption and the visual content.
- SRA (Spatial Relation Accuracy):** Evaluate whether the relative positioning (e.g., left/right, top/bottom, foreground/background) and the logical perspective between multiple instances are accurately depicted in the image.

#### # CRITICAL SCORING RULES (Must Strictly Follow):

- Hierarchical Dependence:** **IEV** is the gatekeeper. If any critical instance is missing (IEV below 4), the corresponding AAA and SRA for the image must be penalized accordingly, as attributes and relations cannot exist without the entity.
- Detail Awareness:** Since this is a high-resolution image evaluation task, you must meticulously scan **the entire canvas**, including corners and background, to identify all mentioned instances and their micro-details.
- Strict Adherence to Explicit Constraints:** Judge the image **ONLY** based on what is explicitly stated in the long caption. Do not impose imaginary constraints or personal aesthetic preferences. For any visual aspects **NOT** mentioned (e.g., specific lighting, background nuances, or artistic style), the generation model is allowed creative autonomy. Do not penalize the model for "making choices" where the prompt is silent.
- Hallucination Penalty:** If the synthesized image contains prominent instances that are **NOT** mentioned in the long caption and significantly distract from the caption's content (severe hallucination), deduct 1-2 points from **IEV**.
- No Middle Ground Bias:** Avoid giving 7/10 by default. Be decisive based on the visual evidence.
- Objectivity & Fairness:** Maintain an objective stance throughout the evaluation process and base your judgement on visual evidence with the same standard instead of subjective preference.

#### # SCORING RUBRICS (10-Point Scale):

##### ## 1. IEV (Instance Existence Verification)

- [9-10]:** All instances (primary and secondary) from the long caption are present and clearly identifiable in the image. No significant omissions.
- [7-8]:** Primary instances are present; only minor, non-essential background elements are missing or extremely unclear.
- [5-6]:** At least one primary instance is missing, or multiple instances are severely obscured; but the image still captures the general theme and content of the caption.
- [3-4]:** Multiple primary instances are missing or unrecognizable, significantly detracting from the caption's description.
- [1-2]:** Total mismatch; the image fails to depict the core content of the caption.

##### ## 2. AAA (Appearance Attribute Alignment)

- [9-10]:** Perfect alignment. All visible attributes (color, texture, material, size, shape) of the instances matches the caption exactly.
- [7-8]:** Most attributes are correct; slight deviations in secondary details (e.g., shade of color or minor texture mismatch) that do not significantly affect the overall perception.
- [5-6]:** Noticeable attribute misalignment in primary instances (e.g., wrong color or material), but the image still somewhat reflects the caption's content.
- [3-4]:** Severe attribute misalignment; primary instances look totally different from the text description.
- [1-2]:** Complete attribute failure; objects lack any descriptive fidelity or are rendered as generic blobs.

##### ## 3. SRA (Spatial Relation Accuracy)

- [9-10]:** All relative positions between instances and depth cues perfectly match the spatial prepositions in the caption.
- [7-8]:** Relative positions are correct, but there are minor errors in scale/perspective or overlapping logic that do not cause major confusion.

- **[5-6]:** Noticeable spatial relation errors (e.g., left/right flipped, foreground/background confusion).
- **[3-4]:** Obvious spatial relation failures; instances are positioned in a way that contradicts the caption's logic.
- **[1-2]:** Chaotic layout; objects are floating or positioned randomly without regard for the caption's logic.

# OUTPUT RULES (Must Strictly Follow):

1. You MUST follow a strict 10-point scale and provide a score as an **INTEGER** from 1 to 10 only for each dimension.
2. Provide the final output strictly **in** a JSON object inside the `<json>` tag.
3. The `<json>` block MUST contain ONLY the valid JSON object. No markdown code blocks or extra text.
4. Keys: "reasoning", "IEV", "AAA", and "SRA". "reasoning" is a concise explanation justifying the scores; "IEV", "AAA", and "SRA" represent the scores for the 3 dimensions respectively. Ensure the JSON property names are enclosed in double quotes and there are no trailing commas in the JSON object.

**Output example for reference (do not copy this exact content, just an example of the structure):**

`<json>`

`{`

`"reasoning": "The cat and the bench is present but the straw hat is missing; the absence of the hat results in a deduction in IEV. The cat's color and texture are reasonably well-aligned with the caption, though the fur appears more orange than described, leading to a moderate AAA score. The spatial relations are mostly accurate, with the cat sitting on bench and positioned on the left as specified, but the background elements are somewhat jumbled, resulting in a high but not perfect SRA score.",`

`"IEV": 6,`

`"AAA": 8,`

`"SRA": 9`

`}}`

`</json>`

Now, please evaluate the **instance-centric compliance** of the provided image based on the above criteria and output the scores and reasoning in the specified **JSON** format.



**Figure A5** One qualitative  $15289 \times 8600$  sample in our PixVerve-95K dataset.



**Figure A6** One qualitative 11656×8742 sample in our PixVerve-95K dataset.